æ

15. CYTOSKELETON, CELL SHAPE, AND MOTILITY

4 August 2019

Essentially all cells engage in activities that require molecular movement, beyond that afforded by diffusion. Familiar forms of cell motility involve the activities of flagella or pseudopodia. However, various modes of internal cellular movement, especially in eukaryotes, are required for the transport of large cargoes, such as vesicles, and cell division requires activities that deform membranes. Central to all of these cellular features are protein fibrils comprised of long concatenations of monomeric subunits, which act dynamically by growth and contraction. In eukaryotes, such proteins serve as highways for the movement of special cargo-carrying molecular motors that effectively walk by use of fuel provided by ATP hydrolysis. Fibrillar proteins are also essential for maintaining cell size and shape, and in eukaryotes, they form the core of motility processes for swimming and crawling.

This chapter continues our narrative on the internal anatomy and natural history of cellular components, exploring the evolutionary diversification of cytoskeletal proteins and their varied functions, as well as the expansion of diverse sets of eukaryote-specific molecular motors and their roles in intracellular transport. It will become clear that filament-forming proteins are at least as diverse in prokaryotes as in eukaryotes, playing central but contrasting roles in structural support and cell division. The limits to motility of single-celled organisms will be shown to follow some general scaling laws across the Tree of Life. Although prokaryotes and eukaryotes both use flagella to swim, and such structures are sometimes suggested to be so complex as to defy an origin by normal evolutionary processes, it turns out that the flagella in the two groups evolved independently and operate in completely different manners, with plausible routes of emergence involving modifications of pre-existing cellular features. Less clear is how cell division and motility was carried out prior to the origin of filaments.

The Basic Cytoskeletal Infrastructure

Three major groups of fibrillar proteins exist across the Tree of Life. Although the most celebrated members, actins and tubulins, are often viewed as eukaryotic innovations, relatives of both families exist in various prokaryotic lineages, where the functions (cell-shape sculpting, cell division, plasmid replication partitioning,

and magnetosomes) are at least as diverse as in eukaryotes (Ozyamak et al. 2013). This phylogenetic distribution suggests that ancestors of most of the major fibril-forming proteins were present as early as LUCA. How motility and cell division were carried out prior to the origin of filaments is unknown, but the emergence of self-assembling fibrils would have been a watershed moment for evolution, by providing opportunities for new intracellular structural environments.

All filaments are comprised of chains of monomeric subunits. As with many other cellular innovations in eukaryotes, gene duplication followed by divergence has often led to subfunctionalization and neofunctionalization of these subunits. Nonetheless, despite their substantial sequence divergence, monomeric secondary structures are often maintained to such a degree that fibrillar proteins from very distant species can function in novel host species (Horio and Oakley 1994; Osawa and Erickson 2006). General reviews can be found in Wickstead and Gull (2011), Erickson (2007), Michie and Löwe (2006), and Löwe and Amos (2008). It bears noting that a number of filament-forming proteins not discussed below are sequestered in various prokaryotic lineages (Wagstaff and Löwe 2018). This supports the idea that fibrils are not particularly difficult to evolve, the main requirements being the emergence of a heterologous interface and a presumed selective advantage (Chapter 12).

Actins. One of the most abundant proteins within eukaryotic cells, actin filaments are homopolymeric, double-stranded, and helical, typically 5 to 9 nm in diameter (Figure 15.1). Free actin monomers are generally bound to ATP, and upon joining a filament gradually undergo ATP hydrolysis. Actin filaments are polar, with the monomeric subunits being added at the plus (barbed) end. Combined with removal at the minus end, this can result in the "apparent" movement of a filament in a treadmilling-like process (Carlier and Shekhar 2017) – at a critical concentration of monomers, the end-specific rates of addition and removal will be equal, with no net filament growth and simple movement of the ends. At least eight families of actin-related proteins (ARPs), related to actins by gene duplication, are involved in the nucleation of new filaments and patterning of branches off parental actins (Goodson and Hawse 2002).

Actins play diverse roles in eukaryotic cells, including involvement in the formation of the cell cortex, vesicle trafficking, cell division, endocytosis, and amoeboid movement. Multiple families commonly exist within a species, with different copies often being assigned to different intracellular functions (e.g., Sehring et al. 2006; Joseph et al. 2008), although *S. cerevisiae* encodes only a single copy. Despite their diverse functions, actins are among the most conserved eukaryotic proteins at the amino-acid sequence level.

Actin-like proteins in bacteria share the basic structural architecture of eukaryotic actin (including the ATP binding site involved in polymerization/depolymerization and the contact sites at monomer interfaces) and are therefore likely phylogenetically related (Ghoshdastider et al. 2015), but they are substantially different sequence-wise (sometimes to the point of not being identifiable by this means; Bork et al. 1992). The bacterial actin relatives also have diverse functions, but are sporadically distributed over the bacterial phylogeny, usually with only one or two types per species. MreB is involved in the maintenance of rod-shaped cells, forming helical

shapes around the cell periphery (Margolin 2009). ParR acts like a centromeric-binding protein, elongating and pushing plasmid copies to the opposite ends of the dividing parental cell with a concatamer of ParM (Salje et al. 2010). In some bacteria, magnetite crystals organize along a MamK filament, creating a magnet used in orientation (Bazylinski and Frankel 2004). Expression of DivB in foci during times of stress induces *Streptomyces* to grow into branching, filamentous mats. Although usually consisting of double-stranded helices, these broad families of bacterial filaments vary widely with respect to the periodicity of twists, the degree of staggering between strands, and even the direction of helix winding (handedness). A protein harbored by the archaebacterium *Pyrobaculum calidifontis,* crenactin, has closer sequence similarity to eukaryotic actins and again shares similar helical structure (Ettema et al. 2011; Braun et al. 2015; Izoré et al. 2016).

Tubulins. The second major types of eukaryotic filaments are tubulins, which initially assemble into thin protofilaments through the stepwise addition of heterodimers of α- and β-tubulin subunits. These fibrils are, in turn, bundled into microtubules – hollow cylinders consisting of 13 protofilaments, approximately 25 nm in diameter (Figure 15.1). Unlike actins, which use ATP hydrolysis in assembly, tubulins use GTP hydrolysis. The minus ends of microtubules are generally anchored at a microtubule-organizing center, such as a centrosome, a spindle-pole body, or a basal body. Growth and contraction occurs at the opposite end in a process known as dynamic instability, which plays a central role in various aspects of cell motility and spindle formation during cell division (Gardner et al. 2013; Akhmanova and Steinmetz 2015).

α- and β-tubulin are products of an ancient gene duplication that preceded LECA, but as in the case of actins, tubulins clearly underwent additional rounds of gene duplication on the road from FECA to LECA. In addition to the α and β subfamilies, at least six other distinct families are known in eukaryotes (although only γ seems to be present in all lineages), and these are generally deployed in different cellular contexts, e.g., basal bodies out of which cilia and flagella grow, rails for vesicle transport, and mitotic/meiotic spindles used for chromosome separation. Such diversification of function, sometimes called the multi-tubulin hypothesis (McKean et al. 2001; Dutcher 2003), extends to different variants within the α and β subtypes. Consider, for example, two closely related amoeboid protists, which exhibit extreme forms of pseudopodia: foraminiferans produce branching networks (reticulopodia) that assist in prey capture, whereas radiolarians produce stiff, spine-like axopodia that assist in floating and capturing prey. In addition to the conventional β tubulin, each group deploys a modified β type to construct the unique helical filaments involved in such structures (Hou et al. 2013).

Again as with actins, there is clear evidence that the antecedents of tubulins were present in LUCA, the most telling of which is FtsZ, a protein that assembles into homomeric filaments that can form bundles (but not organized microtubules), with the monomeric subunits having nearly identical structures to those of tubulin despite very low sequence identity (Löwe and Amos 2009). The few sites that are conserved between tubulin and FtsZ are almost all involved in GTP binding. FtsZ produces contractile rings that guide bacterial cell division, although at least one bacterial group (the planktomycetes) deploys an unrelated protein for such purposes

(Van Niftrik et al. 2009). FtsZ-related proteins are also present in eukaryotes, where they form the division ring responsible for fission of mitochondria and chloroplasts (both of which are ultimately derived from bacterial lineages; Chapter 22). Such proteins have, however, been lost from a number of eukaryotic lineages (including metazoans), implying alternative modes of organelle division (Kiefel et al. 2004; Bernander and Ettema 2010).

Most eukaryotes harbor a pair of barrel-shaped organelles called centrioles, comprised largely of microtubules. With few exceptions, each of these consists of a ring of nine microtubule triplets surrounding two centrally located triplets, with the overall structure resembling a cartwheel. Centrioles serve as the basal body from which flagella and cilia grow (below), and given their distribution throughout eukaryotes (with losses in a few lineages, including yeasts and land plants), it appears that they were present in the ancestral eukaryote (Carvalho-Santos et al. 2010, 2011; Hodges et al. 2010). In animals and some fungi, centrioles play a second role, comprising the centrosome that serves as the organizing center from which the mitotic spindle expands during cell division (Chapter 6). Much of our knowledge of centrosome biology derives from studies of animals, where during sexual reproduction the centriole is excluded from the egg and introduced via the sperm, possibly an evolutionary outcome of sexual conflict and/or sperm competition (Ross and Normark 2015), which may be causally related to the high rate of evolution of centriolar protein sequences (Carvalho-Santos et al. 2011). Some insects have evolved centrioles with much more elaborate structures than the conventional nine-triplet cartwheel, and a few protists have simpler structures (Gönczy 2012), although the mechanisms driving such change remain unknown.

Although the 13-protofilament microtubule architecture appears to be unique to eukaryotes, related structures do exist in some prokaryotes. For example, some members of the Verrucomicrobiales genus *Prosthecobacter* contain two tubulin-like genes, BtubA and BtubB, that form heterodimers, which in turn polymerize into five-filament microtubules capable of dynamic instability (Pilhofer et al. 2011; Deng et al. 2017). Acquisition by horizontal transfer from a eukaryote cannot be ruled out, but regardless, the altered assembly clearly indicates the potential for variation in microtubule structure. The general picture is that FtsZ and the tubulins are all members of a common family of proteins, with the ancestor to the lineage containing tubulins and BtubA/B having evolved a heterodimeric form after gene duplication, as the two duplicates are more closely related to each other than to FtsZ.

One of the more interesting aspects of actin and tubulin-related proteins is that they have seemingly exchanged roles in cell division in eukaryotes vs. prokaryotes. Cytokinesis involves a tubulin-like ring (FtsZ) in bacteria but an actin ring in eukaryotes. In contrast, microtubules are used to move chromosomes apart in eukaryotes, but actin-like molecules are involved in the partitioning of plasmid genomes in bacteria. Notably, different phylogenetic subgroups of the archaea appear to deploy diverse sets of filaments in cytokinesis, some FtsZ-like and others actin-like (Makarova et al. 2010).

As will be noted in the next section, actins and tubulins act in consortia with motor proteins to accomplish a wide array of intracellular functions. However, these fibrils are also capable of work on their own, resulting in pushing forces that can be used to move various organelles and to deform the cell membrane. How can this

occur if the fibrils grow at the tips that are in contact their targets? Although not all of the details are worked out, it appears that continued fibril elongation occurs by a sort of Brownian motion ratchet. Slight fluctuations at points of contact allow occasional room for a new monomer to join the pushing end of the fibril, thereby ratcheting the point of contact forward.

Intermediate filaments. A third group of fibril forming proteins known as intermediate filaments are quite unlike tubulins and actins structurally. They form unpolarized cables and sheets and are not dynamic. Although they are assembled from dimeric subunits, these are in the form of coiled coils, which generally assemble into higher-order structures such as sheets (Figure 15.1). Intermediate filaments are mostly confined to metazoans and slime molds, where they have a variety of functions involved in providing structural strength, e.g., lamins, keratins, and desmins (Preisner et al. 2018). This restricted distribution, sequestered to one clade, suggests a post-LECA origin. A potential homolog, crescentin, exists in the bacterium *Caulobacter crescentus* and is thought to determine cell shape.

Foundations 15.1. The eukaryotic cellular investment in the cytoskeleton. Given the central roles that the cytoskeletal proteins, actin and tubulin, play in eukaryotic cell biology, it is of interest to evaluate the fraction of the cell's energy budget devoted to their production. Estimates are available for the average number of monomers of each protein within the cells of a few species, and this information combined with the cost of protein biosynthesis (to be covered in more detail in Chapter 16) and the cost of building an entire cell (Chapter 4) can be used to obtain a rough estimate of the relative cost of the cytoskeleton.

For the two model yeast species, the average numbers of actin and tubulin monomers per cell are: $88,600$ and $22,400$ for *S. cerevisiae* (Norbeck and Blomberg 1997; Kulak et al. 2014); and $731,500$ and $125,100$ for *S. pombe* (Wu and Pollard 2005; Marguerat et al. 2012; Kulak et al. 2014). Together, these account for just $\sim 0.24\%$ and 0.77% of the total number of proteins per cell in these species.

These numbers can be converted into bioenergetic-cost estimates by noting that: 1) actin and tubulin monomers contain ~ 375 and 450 amino acids, respectively; and 2) the average cost of biosynthesis is 3 ATP hydrolyses per amino acid, with another 4 hydrolyses necessary for polypeptide-chain elongation. Taking the total cost to be the product of the number of monomers, the number of amino acids per monomer, and 7 ATP hydrolyses per amino acid leads to total costs of 2.3×10^8 and 7.1×10^7 for actin and tubulin in *S. cerevisiae,* and 1.9×10^9 and 3.9×10^8 in *S. pombe.* There are additional costs associated with transcription and with maintaining the actual genes, but as will be more fully discussed in Chapter 16, about 90% of the cost of running genes is associated with protein production, so the above numbers are only slight underestimates.

To put this into broader perspective, recall that Equation (4.2b) yields an estimate of the cost of building an entire cell, given the cell volume, which is $\sim 70\,\mu\text{m}^3$ for *S. cerevisiae* and $130\,\mu\text{m}^3$ for *S. pombe.* The number of ATP hydrolyses required for the construction of cells in these two species is then $\sim 1.5 \times 10^{12}$ and 2.9×10^{12}, respectively. Thus, just 0.02 and 0.08% of the total energy budgets for cell construction in these species is devoted to the cytoskeleton, with $\sim 75\%$ of those costs being associated with actin. Similar calculations for data from mouse fibroblast cells (Schwanhäusser

et al. 2011) leads to estimates of 0.8% for actins and 0.4% for tubulins, and for human HeLa cells (Kulak et al. 2014) of 0.02% for actins and 0.1% for tubulins.

It is of interest to note that the two major cytoskeletal proteins in *E. coli,* FtsZ and MreB, have averages of $3,450$ and $1,060$ protein monomers per cell (Pla et al. 1991; Rueda et al. 2003; Lu et al. 2007; Taniguchi et al. 2010; Wizniewski and Rakus 2014; Vischer et al. 2015; Ousounov et al. 2016; Bratton et al. 2018), with respective contents of 383 and 347 amino acids/monomer. With the cost of building an *E. coli* cell of $\sim 27 \times 10^9$ ATP hydrolyses (Chapter 4), the fractional contributions of these two molecules to the total cell budget are 0.034 and 0.010%, respectively. Thus, although the common view is that eukaryotes invest substantially more in cytoskeletal infrastructure than do prokaryotes, this simple comparison between yeasts and *E. coli* suggests an increase in the former of just $\sim 2\times$.

Molecular Motors

Most of the intracellular molecular transport in prokaryotes is passive, driven primarily by diffusion generated by background thermally driven molecular motion. A key innovation in eukaryotes is active transport driven by ATP-consuming mechanisms. Emerging on the path between FECA and LECA is a set of molecular motors with diverse functions ranging from cargo transport along actin filaments and microtubules to the movement of flagella. There are three major families of cytoskeletal motors – dynein, kinesin, and myosin – all of which appear to be eukaryote-specific, and together supplement the cytomotive capacity of the cytoskeletal filaments. Actins and tubulins can exert mechanical pressure as they push against larger structures, and thermal fluctuations allow the stochastic insertion of monomeric subunits and progressive extension. Motor proteins engage in additional work by interfacing between filaments and other structures (including other filaments) and dragging along their cargos (Figure 15.2).

Myosins travel exclusively on actin filaments, whereas kinesins and dyneins operate on microtubules (tubulin filaments). Although their physical structures vary, each type of molecule works by the same mechanism – the transduction of chemical energy into mechanical force via ATP hydrolysis. Effectively, the molecules walk along their cytoskeletal roadways, with each ATP hydrolysis resulting in one step forward (in some cases two hydrolyses occur per step; Zhang et al. 2015). Each motor molecule has an ATP-binding site, a track-binding site, and a tail domain involved in attachment to cargo.

Ubiquitous to all eukaryotes, kinesins underwent massive diversification into an estimated eleven families prior to LECA (Lawrence et al. 2004; Wickstead et al. 2010). Prominent roles include vesicle transport, spindle assembly and chromosome segregation, and intraflagellar transport of flagellar components. Monomeric, dimeric, trimeric, and tetrameric forms exist, and the multimers may be either homomeric or heteromeric. The motor domains operate like walking feet and are generally paired at one end of the molecular structure, although tetramers have motor domains on both ends. Kinesin movement is generally unidirectional, towards

the "plus" ends of microtubules (usually from the center to the edges of cells), with rates of movement on the order of 1 μm/sec (Scholey 2013). Different kinesins have different neck lengths, which determine the degree of processivity of the motors long tubulin filaments (Hariharan and Hancock 2009; Shastry and Hancock 2010), although the degree to which such variation has been molded by selection remains unknown.

Myosins are nearly ubiquitous among eukaryotes, but apparently have been lost from red algae, diplomonads, and trichomonads (Richards and Cavalier-Smith 2005; Foth et al. 2006). The most likely ancestral state prior to eukaryotic diversification is something on the order of three classes, all derived from a single common ancestral protein en route from FECA to LECA. Like kinesins, myosins have diversified into a large number of classes (as many as 24; Foth et al. 2006; Goodson and Dawson 2006), again with numerous functions, including cellular motility and transport of organelles, vesicles, and mRNAs. An argument has been made that diversification of functions followed paths of subfunctionalization, from generalized to more specialized forms (Mast et al. 2012), with the original functions involving cytokinesis, vesicle transport, phagocytosis, and locomotion by pseudopods. Although most myosins are dimeric with parallel coiled-coil domains, monomeric forms exist, as do dimers with anti-parallel constructs with actin-binding domains at each end (Quintero and Yengo 2012). Almost all myosins move in the + direction of actin filaments, although a few are known to move in the opposite direction. Each type of molecule has a particular level of affinity for filaments and a particular step length (usually 5 to 40 nm per step), which together determine the speed of movement. Myosin and kinesin may have evolved from a common ancestor – although they differ in size and exhibit little sequence similarity, their functional domains have highly similar 3-D structures (Kull et al. 1998).

The third major class of motor proteins, dyneins, have a substantially different structure than kinesins/myosins, including an intramolecular hexameric ring consisting of AAA (ATPases Associated with cellular Activities) domains, all physically linked in a single gene (most other AAA proteins are homohexamers constructed from separate polypeptide chains) (Kardon and Vale 2009). As a consequence of this structure, dyneins typically contain > 4500 amino-acid residues, placing them among the largest known proteins. Contrary to the situation with kinesins, dyneins always walk towards the – ends of microtubules, typically towards the cell center. Although they do share the attribute of having two walking feet, with each step fueled by single ATP hydrolyses, unlike the case in kinesins, the steps do not always proceed in a coordinated fashion (Walter and Diez 2012). In total, there are at least nine deeply diverging dynein lineages, most of which trace back to LECA, but dyneins are also unique in that all but one cytoplasmic family member is associated with the cilium (Wickstead and Gull 2007; Wilkes et al. 2008). These axonemal dyneins operate in a team-like fashion to elicit ciliar movement, causing microtubules to slide past each other. Dyneins are ubiquitous across the eukaryotic tree, although they were independently lost in the lineages leading to land plants and red algae.

Although molecular motors have been subject to numerous biochemical and biophysical studies, major evolutionary questions have gone unasked. The three central phenotypic features of motor proteins are their step length, step rate, and

processivity (distance progressed before falling off their substrate). The rate of movement is equal to the product of the step length and rate, yet we know very little as to how these traits vary among species or motor family members within species.

Motility

All cells are capable of movement, even if simply as a consequence of the physical forces associated with cell division. Here, however, the concern is with active movement within the lifespan of a cell, as in swimming or crawling. The range of motility mechanisms is diverse, and even seemingly similar, complex mechanisms such as flagella have evolved independently in different lineages. Regardless of the mechanism, almost all forms of motility require some investment of energy, either a gradient of hydrogen ions driving a turbine-like apparatus or active hydrolysis of ATP used in the conversion of chemical to mechanical energy. In addition, the construction of the motility machinery itself can require a substantial energetic investment. The implication then is that unless active motility provides a boost in fitness, the mechanism will be liable to rapid loss.

The details of how simple cells can utilize mechanisms of directed motion to enhance resource acquisition will be addressed in Chapter 17, with the primary focus here being on the evolutionary origins of motility machineries and the costs of running and building them. Most attention will be given to flagella and cilia, the primary drivers of locomotion in cells in aquatic settings, as these have received considerably more attention than mechanisms of crawling. Even here, it is necessary to give separate consideration to prokaryotes and eukaryotes as the flagellar machineries in these two groups are not only unrelated but operate in fundamentally different ways.

Prokaryotic flagella. Although the primary focus here is on movement by use of flagella, it is worth noting that a number of less well-understood mechanisms of bacterial motion, including movement on solid surfaces, are known (Jarrell and McBride 2008; Nan and Zusman 2016). For example, some bacteria, such as *Neisseria,* are capable of crawling over surfaces by twitching of Type IV pili, whereas others, such as the social bacterium *Myxococcus,* glide by use of surface adhesins (either secreted or embedded in the membrane), and still others move by an inchworm-like mechanism involving membrane-embedded proteins. Some planktonic cyanobacteria, such as *Synechococcus,* can swim without flagella (Waterbury et al. 1985), and others are capable of buoyancy regulation via gas vacuoles (Walsby 1994).

The flagellum represents one of the most complex molecular machines within bacterial cells (Figure 15.3). The dozens of proteins contributing to the overall structure can roughly be divided into five major components: the basal body (which includes the membrane-embedded stator within which the motor rotates), the switch, the hook, the filament, and the export apparatus. Flagellar assembly starts at the basal body, anchoring the overall structure to the cell membrane, proceeds to the construction of the hook, and finally to the filament. The latter is a hollow, tubular structure, consisting of tens of thousands of flagellin molecules, making this one of

the most abundant proteins in a bacterial cell. Its assembly proceeds by the export of component proteins through a central pore. Specific chaperones are assigned to each exported protein, which have to remain unfolded until passing through the pore. The monomeric flagellin subunits are configured in such a way that the final structure is helical in form. Unicellular species live in a low Reynold's number world (Foundations 16.2), with essentially no inertia upon cessation of activity. Rather than pushing the cell forward like legs or wings on an animal, flagella essentially operate like cork screws, dragging the cell forward through the effectively syrup-like environment.

Driven by a proton-motive force (or in some cases, by a sodium-motive force), the helical filament rotates within the hub embedded in the cell membrane, operating like a screw to pull the cell forward (Manson et al. 1977, 1980; Meister et al. 1987). Although the bacterial flagellum does not directly consume ATP, an ATP-driven proton pump maintains the gradient of hydrogen ions necessary to run the turbine. Energy associated with the entry of ions in the intermembrane area (bacteria have two cell membranes) through channels surrounding the motor is converted to a rotational force, which is applied to the internal shaft, analogous to the links of a bicycle chain rotating a wheel. The speed and orientation can be regulated through various signal transduction systems (Chapter 21) that modify the action of molecular brakes (Boehm et al. 2010).

Despite the intricacies of the bacterial flagellum, there is substantial phylogenetic variation in its basic features, including left- vs. right-handedness, the angularity and periodicity of the helices, clockwise vs. counter-clockwise rotation of the helices (or both), the number of distinct flagellin proteins incorporated into the filament, the number of protofilaments per flagellum, and the number of stators per basal body (Pallen and Matzke 2006; Galkin et al. 2008; Chaban et al. 2018; Kaplan et al. 2019). Enormous variation also exists in the structure and number of components in the basal body (Chen et al. 2011; Chaban et al. 2018; Rossmann and Beeby 2018). The cellular positions (from polar to lateral) and numbers of flagella can also be highly variable. In spirochaetes, the flagella are not even external, but reside with the periplasmic space, where their twisting contorts the entire cell. Such features must influence the efficiency of conversion of chemical to mechanical energy, but comparative studies essential to understanding the phylogenetic distribution of such variation remain to be done. The degree to which the scattered presence of flagella throughout the bacterial phylogeny is due to lineage-specific losses or gains by horizontal gene transfer remains unclear (Snyder et al. 2008).

How might a molecular machine as complex as a bacterial flagellum have arisen? The logical hypothesis is that paths of descent with modification are involved, and some evidence supports this. The entire system appears to be related to bacterial Type-III secretion systems (Pallen et al. 2005), which are used to transfer infection-determining proteins into host cells. At least ten components of such systems have strong homologies to components of the bacterial flagellum, and the overall structure is similar in architecture and function, except that instead of a flagellum, the secretion system harbors a stiff injection apparatus (Blocker et al. 2003; Egelman 2010). In addition, the subcomponent that drives flagellar component export is related to the catalytic subunits of ATP synthase. Less clear is whether the flagellum is a derived Type-III secretion system or vice versa.

Liu and Ochman (2007) provide evidence that of the greater than 50 genes whose products enter the bacterial flagellar system, 24 were likely present in the common ancestor to all bacteria, and that even among these, many of the component origins involved gene duplication. They further suggest that the order of inferred duplications imply an "inside-out" sequence of evolutionary steps that in turn reflects the assembly process, i.e., basal body, hook, junction, filament, a potential example of ontogeny recapitulates phylogeny. If correct, this implies that the flagellum arose from something like a Type-III secretion system, rather than the other way around. However, just as the flagellum may have evolved from bacterial structures with alternative functions, loss of the flagellum sometimes leads to the maintenance of basal structures with presumed alternative functions. For example, *Buchnera aphidicola,* an endosymbiont that inhabits the cells of aphids, has lost the flagellar filament, but the cells still harbor hundreds of hook/basal body structures, with likely roles in secretion into host cells, much like Type-III secretion systems (Maezawa et al. 2006; Toft and Fares 2008).

Although fairly similar in overall structure, the flagella of archaea appear to be completely unrelated to those of bacteria, providing a remarkable example of convergent evolution. As in bacteria, the archaeal flagellum (the archaellum) rotates via an embedded membrane structure, but the protein components appear to be nonhomologous to those found in bacteria. Moreover, rather than being driven by a proton-motif force, ATP hydrolysis drives rotation of the archaellum (Thomas et al. 2001; Desmond et al. 2007; Lassak et al. 2012; Daum et al. 2017; Albers and Jarrell 2018). Unlike bacterial flagella, archaeal flagella are not hollow, and they have no hook structure, with assembly occurring at the base rather than at the distal tip. The components of the whip, archaellins, appear to be unrelated to flagellins. Archaeal flagella appear most closely related to bacterial type IV pilus systems (Albers and Pohlschröder 2009), which are used as adhesive structures and in twitching motility, although this too might be a matter of convergence.

Eukaryotic flagella. This theme of diversity extends to the eukaryotic flagellum, which is unlike anything utilized in the prokaryotic world, having no protein components that are obvious prokaryotic orthologs. Moreover, unlike the rotational flagella of prokaryotes driven by a proton-motive force, eukaryotic flagella operate by an undulatory mechanism driven by ATP consuming processes, although there are many variants on this theme. For example, the green alga *Chlamydomonas* can swim either by a breaststroke or by undulatory waves (Tam and Hosoi 2011). The cryptophyte *Ochromonas* has perpendicular hairs (mastigonemes) radiating from the flagellum, creating a feather-like appearance. Combined with the use of flagella, euglenoids are capable of additional cell contortions (called metaboly), with the cell shifting the positions of cellular contents in a progressive way along its axis (like food moving through the body of a boa constrictor). In trypanosomes, a single flagellum is embedded along the side of the cell. The word cilia (singular cilium) is generally reserved for short oar-like flagella that coat large or entire portions of the cell surface, as in ciliated protozoans. In all cases, eukaryotic flagella/cilia are driven by motor proteins, which cause the core doublets of microtubules to slide past each other. Only a few lineages have lost the ability to produce flagella, most notably slime molds, yeasts, some phytoplankton, and most land plants, and the

general conclusion is that the origin of the cilium preceded LECA (Cavalier-Smith 2002).

Eukaryotic cilia are much larger than bacterial flagella, generally on the order of 200 nm in diameter, and almost always consisting of bundles of nine peripheral microtubule doublets surrounding a central pair (Ginger et al. 2008; Ishikawa and Marshall 2011, 2017). (The central pair is typically absent in primary cilia used purely as sensing organs in cells of metazoa). This overall core structure is known as an axoneme, which remains surrounded by an extension of the cell membrane. The doublets grow out of tubulin-based cylinders known as basal bodies, where the microtubules consist of triplets comprised of δ- and ϵ-tubulins, which arose by gene duplication prior to LECA (Dutcher 2003). In most organisms, the basal bodies are recycled centrioles, which are also used as mitotic organizing centers during cell division. Although the overall structure of centrioles is conserved across the tree of eukaryotes, there is lineage-specific variation in various architectural features (Carvalho-Santos et al. 2011).

While bacterial flagella are comprised of a few dozen proteins, on the order of 250 to 500 proteins contribute to the eukaryotic flagellum (Avidor-Reiss et al. 2004; Pazour et al. 2005; Smith et al. 2005). For the few organisms for which the flagellar proteome has been evaluated (the green alga *Chlamydomonas,* the ciliate *Tetrahymena,* and mammals), ~ 200 proteins are flagellar-specific and not found in nonciliated species (Avidor-Reiss et al. 2004; Smith et al. 2005).

Numerous activities occur within the lumens of eukaryotic flagella, which are in a constant state of assembly and disassembly at the tip. As there are no ribosomes within the flagellum, all materials must be selectively imported by intraflagellar transport (IFT). Kinesins move structural and other flagellar components forward on one member of each doublet, while dyneins move cargo in the opposite direction on the other member (Stepanek and Pigino 2016). As with a two-lane highway, bi-directional traffic collisions are then prevented. Transport rates are on the order of 1 to 3 μm/sec (Ishikawa and Marshall 2017). As flagella function secondarily as sense organs, they also harbor many signal-transduction systems (environmental sensors that initiate information cascades within cells; Chapter 21). In addition, they contain metabolic machinery for generating ATPs that are presumably used to fuel the molecular motors involved in transport and motility (Ginger et al. 2008).

The most convincing argument for the evolution of the eukaryotic flagellum invokes an autogenous origin, starting as protruding microtubule bundle emanating from a microtubule organizing center (as used in mitotic spindles) (Cavalier-Smith 1978; Jékely and Arendt 2006). The initial structure may have had little to do with motility at all, operating instead as an environmental sensing organ. Eventually an IFT system would have to evolve, along with the ninefold symmetric structure of the axoneme, and the recruitment of molecular motors. Because the microtubules themselves are derived from tubulins, and the motors involved are closely related to those deployed in the cellular interior, such a scenario invokes little more than a series of gene duplication and modification events (Hartman and Smith 2009). An alternative hypothesis postulates an origin via a virus that somehow victimized a host cell in such a way as to become a primitive basal body combined with a cellular protrusion for progeny viral particles (Satir et al. 2007; Alliegro and Satir 2009). The cost of maintaining such a pathogen for the eons required for the emergence of

the complex ciliary structure is problematical for this latter argument.

Further insight into the origins of the components of the ancestral flagellum is derived from observations on the similarity to various structural and functional aspects of the nuclear pore complex and vesicle scaffolding proteins. Fibers at the base of the flagellum may operate like nuclear pore proteins as gateways to admission of appropriate protein cargos for intraflagellar transport, making use of RAN-GTP cycles and importin molecules as in the case of transport through nuclear pores (Rosenbaum and Witman 2002; Dishinger et al. 2010; Kee et al. 2012; see Chapter 14). Notably, the two IFT protein complexes that bind to cargoes (and are in turn dragged by motors) appear to be derived by duplication from a common ancestor related to vesicle-coat proteins (van Dam et al. 2013), which as noted in Chapter 14 are in turn related to the scaffold of the nuclear pore complex. Left unresolved here is whether the nuclear-pore complex preceded the evolution of the cilium or vice versa, but these observations again illustrate how the complex features of cells often evolve by duplication and modification of pre-existing structures rather than by *de novo* establishment.

The eukaryotic flagellum has also served as a model for understanding how size homeostasis is maintained for cellular organelles. Because eukaryotic flagella undergo constant assembly and disassembly of tubulin subunits (Marshall and Rosenbaum 2001), maintenance of a constant length requires that the two rates be equal. An equilibrium length requires that one of the two reaction rates be negatively length-dependent, such that disassembly exceeds assembly above the equilibrium length, and vice versa. Such regulation is supported by experiments in the biflagellated *Chlamydomonas,* showing that when one flagellum is severed, it grows back while the other shrinks until the two equilibrate in length (Ludington et al. 2012). The data suggest that the rate of disassembly is length independent, whereas the rate of assembly declines with cilium length. The latter is accomplished by maintaining a constant number of IFT particles per cilia, so that with constant transport speed, the arrival time of tip components declines with the distance that must be traveled by each particle. To maintain a constant number of IFT particles per cilium, the rate of injection of IFT particles must be inversely related to the length of the cilium, which appears to be the case (Ludington et al. 2013).

The costs of motility. Although many cells can swim, and it is easy to imagine adaptive reasons for doing so, e.g., directive movement towards patchy resources and avoidance of predators, not all cells living in aquatic environments can self-propel. The latter include many planktonic bacteria, diatoms, and green algae. This suggests that the energetic cost of swimming in certain settings may exceed the benefits. Here, an effort is made to obtain a rough estimate of such costs for both the act of swimming and of building the mobility apparatus, and to determine how the evolutionary consequences of such costs scale with cell size.

The power requirement for swimming can be estimated as the work required to move an object (usually assumed to be a sphere, or an alternatively shaped cell suitably transformed to an effective sphere) at a particular velocity (Foundations 15.2). Combining such theory with estimated costs of moving flagella, a number of attempts have been made to estimate the efficiency of swimming in microbes. The universal conclusion is that the conversion of chemical energy into motion is quite

low, averaging $\sim 2\%$: $\sim 0.1\%$ for the ciliate *Paramecium* (Katsu-Kimura et al. 2009); 1.3% for the euglenoid *Eutreptiella* (Arroyo et al. 2012); 0.8%, 1.5%, and 1.4%, respectively, for the green algae *Chlamydomonas* (Tam and Hosoi 2011), *Polytoma uvella* (Gittleson and Noble 1973), and *Tetraflagellochloris mauritanica* (Barsanti et al. 2016); 8% for the archaebacterium *Halobacterium* (Kinosita et al. 2016); and 1% and 5%, respectively, for the bacteria *E. coli* (Purcell 1997; Chattopadhyay et al. 2006) and *Streptococcus* (Meister et al. 1987). Thus, the power requirement for swimming is on the order of $50\times$ that expected based solely on the physics of the process. Brownian-motion jostling of cells, rotational diffusion, helical swimming patterns, and flexibility of the flagellum are among the reasons for this low efficiency.

Despite this low efficiency, it has been suggested that the total cost of locomotion is trivially small (Purcell 1977). For example, based on the cost of actin polymerization, Flamholz et al. (2014) estimated that the crawling motion in goldfish keratocytes consumes $\sim 4\times 10^5$ ATPs/second. Their suggestion that the relative cost of movement is small can be understood by noting from Chapter 4 that the basal metabolic requirement of a vertebrate cell is $\sim 5\times 10^7$ ATPs/second, and that, assuming a one-day cell division time, the cost of building such a cell is $\sim 6\times 10^8$ ATPs/second. Viewed in this way, the cost of crawling in this particular case is on the order of 0.1% of such a cell's total energy budget.

Only a few attempts have been made to estimate the cost of swimming. Raven and Richardson (1984) concluded that the cost of running a flagellum for an idealized dinoflagellate is about equal to the basal metabolic rate, whereas Katsu-Kimura et al. (2009) suggested 70% for the ciliate *Paramecium.* Crawford (1992) estimated that 1 to 10% of ciliate and dinoflagellate total energy budgets are allocated to swimming, whereas Fenchel and Finlay (1983) estimated costs equivalent to $\sim 0.4\%$ of total cellular energy budgets in the cryptomonad *Ochromonas* and the ciliate *Didinium.* There are a number of uncertainties in these estimates, and notably, they do not include the cost of building the apparatus required for motion.

Although fractional energy investments on the order of 0.1 to 1% may seem trivial in an absolute sense, this is not the case from an evolutionary perspective, as such a cost can easily be perceived by natural selection except in tiny populations. As discussed in Chapters 9 and 16, the power of natural selection is almost always sufficient to perceive a cost as low as 0.01%, and hence quite capable of promoting a nonmotile mutant should it have such an advantage (or promoting the reemergence of a flagellum where possible). Thus, it is clear that the cost of swimming is sufficiently large that such a trait exists in an evolutionary "use it or lose it" context.

A more general view of the problem can be obtained from the scaling relationship between swimming velocity (v in units of μm/sec) and cell volume (V in units of μm^3) observed for a wide variety of eukaryotic species, $v = 10.5V^{0.30}$ (Figure 15.4). Noting that the radius of a sphere is $(3V/4\pi)^{1/3}$, this suggests a swimming speed for unicellular eukaryotes of ~ 8.5/sec in units of effective cell diameters, independent of cell volume. Such swimming speeds are comparable to those observed for the larvae of marine invertebrates, which generally fall in the range of 5 to 10 lengths/sec (Chia et al. 1984), and much higher than those for swimming vertebrates (fish, birds, seals, and whales, all of which average in the narrow range of 0.5 to 2.5 m/sec; Sato et al. 2007). The peak speeds of the fastest fish (marlins and sailfish) are ~ 15 body lengths/sec, and the maximum speed for an Olympic swimmer is ~ 2

body lengths/sec.

How much energy does such activity demand? From Equation (15.2.2), it can be seen that the power required for swimming scales with the product of the viscosity of the medium (η), the radius of the cell (r), and the squared swimming velocity (v^2), and to account for the inefficient conversion from chemical energy to motion, this must further be divided by 0.02. Assuming spherical cells, the scaling relationship for eukaryotes in Figure 15.4 implies $rv^2 \simeq 68V$ μm^3/sec^2, suggesting a power scaling that is essentially isometric with respect to cell volume. From Chapter 3, the viscosity of water is 10^{-2} g $\cdot$ cm^{-1} $\cdot$ sec^{-1} (assuming 20° C), and after applying this to Equation (15.2.2) and appropriate changes of units, the average power requirement of swimming is estimated to be $(64 \times 10^{-19})V$ kg $\cdot$ m^2 $\cdot$ sec^{-3}, which has equivalent units of joules/sec (here, cell volume V is in units of μm^3).

To put this in more familiar terms, note that a rough estimate of the energy associated with the hydrolysis of one mole of ATP at physiological conditions is 50 kilojoules. After allowing for Avogadro's number of molecules per mole, the power requirement for swimming in units of ATP molecules hydrolyzed/hour is then $\sim (2.5 \times 10^5)V$. Recalling that average basal metabolic rates also scale isometrically with cell volume, as $\sim 0.4 \times 10^9 V$ ATP hydrolyses/hour (Lynch and Marinov 2015), this suggests a fractional energetic investment in swimming of $\sim 0.06\%$ (assuming the cell is constantly swimming), independent of cell volume, quite a bit lower than the preceding estimates, but still easily perceived by natural selection.

This estimate does not include the cost of building the swimming apparatus. As outlined in Foundations 15.3, the total biosynthetic cost of the proteins comprising an *E. coli* flagellum and its basal protein parts is equivalent to $\sim 23 \times 10^6$ ATP hydrolyses, whereas that for the surrounding lipid membrane is $\sim 132 \times 10^6$ ATP hydrolyses, nearly 6$\times$ that at the protein level.

These rough calculations provide the basis for some conclusions with respect to swimming in bacteria. First, recalling from above that the cost of swimming is $\sim (2.5 \times 10^5)V$ per hour (for eukaryotes, and not much higher for bacteria; Figure 15.4), because the average volume of an *E. coli* cell is $V \simeq 1$ μm^3, and the cell-division time is typically no more than a few hours, most of the cost of swimming is associated with building rather than operating the apparatus. This conclusion remains unaltered by the fact that *E. coli* cells generally harbor several flagella. Second, from Chapter 4, the total cost of building an *E. coli* cell is $\sim 3 \times 10^{10}$ ATP hydrolyses, implying that the bioenergetic cost of a building a flagellum is on the order of 0.5% of the total cellular energy budget, with most of this cost being associated with the lipid covering. There will, of course, be quantitative differences among species after differences in flagellar lengths and numbers and cell shape are accounted for, but the qualitative conclusions just reached are unlikely to change.

Similar calculations for eukaryotes (Foundations 15.3) suggest roughly similar total costs of swimming but considerably different fractional contributions of the component costs. Noting that the volume of a *C. reinhardtii* cell is ~ 200 μm^3, and allowing for a 24-hour cell division time implies an energetic cost of swimming of $\sim 1\times10^9$ ATP per cell life time, whereas the costs of flagellar construction are $\sim 5\times10^9$ ATP hydrolyses for the total protein content and $\sim 2 \times 10^9$ for the lipid membrane (for each of the two flagella). With the total cost of building a *C. reinhardtii* cell being equivalent to $\sim 5.4 \times 10^{12}$ ATP hydrolyses (Chapter 4), the relative costs of

operating and constructing each flagellum are 0.02 and 0.13%, respectively.

Notably, these cost estimates for swimming do not include the additional "opportunity" costs (Chapter 16) associated with diverting metabolic precursors that could alternatively be used to generate energy for other purposes. Thus, it can be concluded that the cost of swimming from an evolutionary perspective constitutes a significant fraction of a cell's total energy budget. For a trait to be maintained evolutionarily, the benefits accrued must offset the total costs of construction and operation. In accordance with this view, many bacteria have evolved mechanisms for selective use of flagella, regulating the expression of the necessary genes for use only in environments providing significant benefits. When confronted with nutrient depletion, some species shed all external features of their flagella, leaving behind just a plugged remnant of the flagellar motor, whereas others cease assembly, leading to a reduction in flagellum number as the cells divide (Ferreira et al. 2019).

Prolonged periods of silencing of such genes would be expected to eventually lead to the accumulation of deactivating mutations (and complete loss of motility), and this presumably explains the absence of flagella/cilia from numerous branches in the Tree of Life. There must eventually be a point at which mutation accumulation is so high that reversion to motility is impossible without horizontal gene transfer. However, a remarkable case of the resurrection of a flagellum was observed in an experimental construct of the bacterium *Pseudomonas fluorescens* engineered to be nonmotile by deletion of a key regulatory gene for flagellar gene expression (Taylor et al. 2015). After just four days of strong selection for motility, the bacteria regained flagella as mutations redirected a regulatory gene for nitrogen assimilation towards the promotion of expression of still intact flagellar genes (albeit at the expense of nitrogen uptake).

Foundations 15.2. The physical challenges to cellular locomotion. A key to understanding the relative advantages / disadvantages of motility in single-celled organisms is the way in which the resistance of a fluid to the motion of an object scales with the size of the object (Purcell 1977). The central concept is embodied in the definition of a dimensionless index known as the Reynolds number and equal to the ratio of inertial to viscous forces,

$$\mathrm{Re} = \frac{\rho v L}{\eta}, \tag{15.2.1}$$

where ρ is the fluid density (g/cm^3), v is the velocity of the object (cm/sec), L is the characteristic linear dimension of the object (which depends on the shape; cm), and η is the fluid viscosity (g/cm·sec). For water, $\eta/\rho \simeq 10^{-2}$ cm^2/sec. Although the source of Equation 15.1 may not be intuitive, the derivation follows from the fact that the inertial force of an object (the numerator in Re) is equal to mass times acceleration, i.e., $(\rho L^3) \cdot (v/t)$, where t denotes time. The viscous force follows from the definition of the coefficient of viscosity (η) as the viscous force per unit area per the velocity gradient (change in velocity per distance), which leads to $\eta \cdot L^2 \cdot (v/L)$. Noting that $(v/t)/(v/L)$ is equivalent to v returns Equation 15.1.

The Reynolds number is a convenient index of the challenges confronted by an object moving in a fluid. When $\mathrm{Re} < 1$, viscous forces dominant, and in the limiting case of $\mathrm{Re} \ll 1$, the motion at any particular moment is essentially independent of all

prior motion. In the latter case, the resistance of the fluid is so great that movement of the object ceases nearly instantaneously if the force of motion is stopped. Almost all aspects of cellular movement are in this low Reynolds number range. For example, as noted above for bacterial motility, v is almost always $< 100\,\mu$m/sec, and most bacterial cells have lengths of order $1\,\mu$m, so given that $1\,\mu\text{m} = 10^{-4}$ cm, Re is on the order of 10^{-4}.

A key definition from physics is that power (the rate of doing work, or equivalently the rate of energy utilization) is equal to the product of force and velocity, $P = F \cdot v$. From **Stoke's Law**, which specifically applies to low Reynolds number situations, the inertial drag force is $F = 6\pi r\eta v$, so

$$P = 6\pi r\eta v^2 \tag{15.2.2}$$

for a sphere with radius r. The formula differs for different shapes (see pages 56-57, Berg (1993) for some approximations; and Perrin (1934, 1936) for more general results), although the scaling with ηv^2 remains. One has to be careful with units here. If F in units of kg-m/sec^2, and v has units of m/sec, then P has units of watts or joules/sec. To determine the total metabolic power required to maintain velocity v, the preceding expression must be divided by the efficiency of conversion of electrochemical energy to directional motion (i.e., the ratio of propulsive-power output to rotary-power input), which in *E. coli* is estimated to be 0.017 (Chattopadhyay et al. 2006). Based on a metabolic scaling argument, Dusenbery (1997) estimates that there is a minimal size limit of ~ 0.8 μm below which there is no advantage to motility, although his arguments ignore the cost of building the motility apparatus.

To determine the potential benefits of swimming in terms of resource acquisition, we first consider the simplest situation in which a cell swims in a particular direction with no direct ability to alter the angle of orientation while on a particular bout. Suppose the cell swims with constant velocity v in a three-dimensional environment, pausing for infintesimally short times after durations of length τ, and then randomly starting off in a new direction, with τ being exponentially distributed. Although the physical length of each individual bout is $v\tau$, because the runs are distributed over three dimensions (Chapter 3), and because the times are exponentially distributed, in which case $\overline{\tau^2} = 2\overline{\tau}$, the mean-squared length of movement per bout is $2v^2\overline{\tau}^2/3$. By definition, the mean-squared deviation of movement is $2Dt$ (Chapter 3), where D is the diffusion coefficient, which after factoring out $2t$ implies $D = v^2\tau/3$ under the assumption that the directions of movement between adjacent steps are uncorrelated.

In contrast to the situation in which the directions of successive travel bouts are uncorrelated, if there is some memory of the process such that successive bouts tend to go roughly in the same direction, we can expect the average distance traveled to increase. If there is a tendency to switch to opposing directions, it will be decreased. Such correlations of movement can be accommodated by dividing the previous expression by $(1 - \overline{c})$, where $\overline{c}$ is the mean cosine of the angle of switching (θ) (Lovely and Dahlquist 1975). If the angle of switching is small, $(1 - \overline{c}) \simeq \overline{\theta^2}/2$. The mean-squared angular deviation $\overline{\theta^2}/2$ is analogous to the mean-squared linear (translational) movement encountered in Chapter 2. By definition then, $\overline{\theta^2} = 4D_r\overline{\tau}$, where D_r is the rotational diffusion coefficient.

Even in the absence of organism-induced directional switching of angles, the jostling of molecules in the fluid will cause rotational diffusion, just as it does in the case of translational movement. In this case, it is known that $D_r = k_BT/(8\pi\eta r^3)$ (Berg 1993; Equation 6.6). This leads to an effective diffusion rate for the swimming cell of

$$D = \frac{v^2\overline{\tau}}{3(1-\overline{c})} = \frac{v^2}{6D_r} = \frac{4\pi\eta r^3 v^2}{3k_BT}. \tag{15.2.3a}$$

From Chapter 2, we know that $k_BT \simeq 4.1 \times 10^{-14}$ cm$^2 \cdot$ g $\cdot$ sec^{-2}, and for water $\eta \simeq 10^{-3}$ g $\cdot$ cm$^{-1} \cdot$ sec^{-1}, so in a freshwater environment

$$D \simeq 10^{12} \cdot r^3 v^2, \tag{15.2.3b}$$

where r and v have units of cm and cm/sec, respectively, yielding D with units of cm^2/sec.

If one then considers a bacterium with typical $r \simeq 10^{-4}$ cm, and $v \simeq 3 \times 10^{-3}$ cm/sec, the effective diffusion coefficient is $D \simeq 10^{-5}$ cm^2/sec. From Figure 3.8, the average diffusion coefficient for a typical anion/cation is also $\simeq 10^{-5}$ cm^2/sec, with that for a protein containing 100 amino acids being $\simeq 10^{-6}$ cm^2/sec. Thus, without direct behavioral modifications of swimming direction, rotational diffusion imposed by the surrounding fluid results in a bacterial cell encountering random resources at a rate at least double that expected for a nonmotile cell, and larger, more rapidly swimming cells will achieve even more.

An ability to respond to local resource abundance can enhance encounter rates by imposing a positive directional bias of movement up a resource gradient and a negative bias of directional movements upon encountering a resource-rich patch, e.g., chemotaxis, as outlined in Chapter 21. Consider, for example, a strong positive correlation of directional movement, $\overline{c} = 0.9$. Applying this to the left-most expression in Equation (15.2a), with a bacterial swimming speed of $v \simeq 3 \times 10^{-3}$ cm/sec and $\overline{\tau} = 1$ sec leads to $D \simeq 3 \times 10^{-5}$ cm^2/sec, whereas $\overline{c} = -0.8$ leads to $D \simeq 2 \times 10^{-6}$ cm^2/sec. Thus, behavioral mechanisms can substantially magnify average levels of resource availability by biasing movement towards resource-rich patches in a heterogeneous environment.

Foundations 15.3. The construction costs of flagella. The cost of building a molecular machine such as a flagellum can be estimated using the general strategy outlined in Foundations 15.1 (with further elaborations on the underpinnings in Chapter 16). For a bacterial flagellum, the biosynthetic costs can be roughly computed as follows. From Berg (2003), an average *E. coli* flagellar filament contains ~ 5340 flagellin protein molecules, each containing 500 amino acids, implying a total investment of $\sim 2.7 \times 10^6$ amino acids. The remaining proteins associated with the basal body, rod, and hook comprise only about 5% of the protein in the flagellum (Sosinsky et al. 1992; Berg 2003), so in total there are $\sim 3 \times 10^6$ amino acids involved. As noted in Foundations 15.1, the total translation-associated cost is ~ 7 ATP hydrolyses per amino acid, and additional costs of genes at the DNA and mRNA levels only inflate these estimates by $\sim 10\%$. This implies a protein biosynthetic cost per *E. coli* flagellum of $\sim 23 \times 10^6$ ATP hydrolyses.

There is an additional cost of wrapping the filament with a lipid membrane. Again, the details underlying the computations here will be given in Chapter 16. The essential points are that with an average *E. coli* flagellum radius and length of 0.01 and 6 μm, respectively, the cylindrical surface area of the flagellum is $\sim 0.4\,\mu$m^2. As the average membrane area occupied by a bacterial lipid molecule is $0.65 \times 10^{-6}\,\mu$m^2, after accounting for the two leaflets of the lipid bilayer, there are an estimated 1.2×10^6 lipid molecules surrounding this flagellum. The biosynthetic costs of lipids are much greater than those for proteins, averaging 110 ATP hydrolyses per lipid molecule, leading to a total biosynthetic cost of the flagellar membrane of $\sim 130 \times 10^6$ ATP hydrolyses.

To extend these calculations to eukaryotes, consider the green alga *Chlamydomonas reinhardtii,* which generally has two flagella with approximate radii and lengths of 0.075 and 20 μm. After accounting for the slightly elevated cost of lipid biosynthesis in eukaryotes, this implies a total membrane cost surrounding each flagellum of $\sim 2.0 \times 10^9$ ATP. Raven and Richardson (1984) estimate there to be $\sim 48,000$

tubulin monomers (each ~ 450 amino acids in length) per μm of flagellum, implying a cost for this major molecule of $\sim 3.0 \times 10^9$ ATP; and there are also ~ 600 of the large motor protein dynein (each $\sim 15,000$ amino acids in length) per μm, implying an additional construction cost of $\sim 1.3 \times 10^9$ ATP. There are numerous other proteins within eukaryotic flagella, including the smaller motor protein kinesin, but their summed number is unlikely to rival that for tubulin and dynein, so the total cost of protein synthesis associated with each *C. reinhardtii* flagellum is $\sim 5 \times 10^9$ ATP, more than double the lipid cost (contrary to the ratio in *E. coli,* but expectedly so, given the lower surface area:volume ratio of the thicker eukaryotic flagellum).

Cell Shape

Cells come in a wide variety of sizes and shapes, supported by structures such as cytoskeletal fibrils and cell walls, the spatial deployment of which is guided by specific indicator molecules. Unicellular eukaryotes often have characteristic shapes, to the point of being used as diagnostics for species identification (as in diatoms and dinoflagellates). Bacteria have a wide range of cell shapes as well (Young 2006), but only small number of shapes are commonly utilized. When confined to constricted settings or forced to bend, bacteria can take on a wide variety of shapes, but upon release to more natural settings, they return to their characteristic shapes (Männik et al. 2009; Amir et al. 2014), demonstrating both a capacity for plasticity and a significant degree of genetic determinism. Most bacteria are either spherical or rod-shaped with an average axial (length:diameter) ratio of 3, with nonmotile cells being spheres more frequently than are flagellated cells (Dusenbery 1998; Young 2006).

In general, the precise evolutionary advantages of alternative cell sizes and shapes are unknown. Some issues with respect to cell size will be explored in Chapter 17, and Dusenbery (1998) has quantified the expected fitness advantages of alternative shapes from a purely biophysical perspective. Based on the known behavior of alternative shapes within fluids for cells of a specific volume, the relative advantages of alternative forms – spheres, oblate spheroids (flat ellipsoids), and prolate spheroids (elongate ellipsoids, close to rods in form) – can be determined with respect to various physical factors. If, for example, there is a premium on increased surface area (as would be the case if this were a key mechanism for enhancing nutrient uptake), disk-shaped bacteria would be expected to be common. However, these are almost never found (one exception being *Haloquadratum,* which forms flat squares).

On the other hand, spheres (with minimum surface:volume ratio) have the highest rate of diffusion through a liquid, so if random dispersal is selectively advantageous, this would encourage such a cell shape. The sedimentation rate of spheres also exceeds that of all other ellipsoids. Up to a $2.4\times$ reduction in sinking rate occurs with a rod-like form, though this maximum effect requires an axial ratio of ~ 30, far beyond what is typically observed in bacteria. Owing to reduced drag, swimming efficiency is greatest for a rod with an axial ratio of 2, but this is smaller than what is typically seen, and the advantage is only $\sim 5\%$.

Why then are rod-shaped bacteria so common? Rods generally grow only in

length (not width), essentially keeping the surface area:volume constant over the cell cycle, thereby giving them a consistent surface area:volume advantage over spheres. Rods may also be advantageous in environments where sheer forces are high, as they are able to attach to solid surfaces better than spheres. Although these and a range of other factors might influence cell-shape evolution in different ways depending on the ecological context, environmental sensing (Chapter 21) may be a general factor contributing to the evolution of elongate cells. Elongate cells have a 100 to 600-fold advantage in the potential to sense the direction of chemical gradients (Dusenbery 1998), e.g., by temporally surveying across a gradient or by simultaneously sensing the environment at both ends of the cell. This advantage is largely a consequence of spheres (of equal volume) being much more subject to rotational diffusion (and hence loss of directionality) than rods. Further details on these matters will be addressed in Chapters 17 and 21.

Cellular dimensions can undergo rapid evolutionary change, and the genetic basis for such change can be quite simple at the molecular level. For example, over a period of just a few years, laboratory cultures of *E. coli* have been found to exhibit increases in cell volume via a single mutation in the actin-like MreB gene (Monds et al. 2014). In this particular study, further exploration of the full range of amino-acid changes at one site generated a range of cell sizes, with an increase in growth rate accompanying an increase in cell volume up to a point. Although this might be taken to imply that natural selection favors large cell size, this then begs the question as to why such increase had not occurred before laboratory culture. Likely, optimal cell size is strongly influenced by the environmental setting, and among other things, laboratory settings remove cells from normal day-to-day occurrences such as predation, desiccation, involuntary movement, etc.

The molecular toolbox for bacterial cell-shape determination also appears to be relatively simple, primarily involving two cytoskeletal molecules (the tubulin-like FtsZ, and the actin-like MreB noted above) and a few interacting proteins for directing their use. Although the complex peptidoglycan walls of bacteria (biopolymeric meshes of sugar-derived molecules cross-linked by peptides) provide support structure (Typas et al. 2012), cell-wall assembly towards a particular form is directed by these other molecules. For rod-shaped cells, MreB and its relatives usually play central roles in setting the cellular dimensions, directing the synthesis of the sidewalls, and operating in spatially restricted manners that ensure uniform width (Margolin 2009; Ursell et al. 2014). As noted above for cell shape, simple manipulation of the protein-coding regions of these genes can elicit radical shifts in cell form, e.g., spheres to rods to long filaments, again demonstrating the ease with which cell shape can evolve (Young 2010).

Although the same molecular machinery may be repeatedly exploited for altering cell shape, even within bacteria similar shapes can be achieved by rather different mechanisms. For example, the two model bacteria *E. coli* and *B. subtilis* both use MreB to maintain their rod shapes, but the helical movement of this molecule proceeds in a left-hand fashion in the former and a right-hand fashion in the latter, and deployment of MreB in wall growth differs, the first species regulating the amount of peptidoglycan loaded per MreB patch and the second the speed of growth of individual MreB patches (Wang et al. 2012). In addition, the two species differ in the ways in which they integrate subunits into the cell wall, the thickness of which

in *E. coli* is only $\sim 10\%$ that in *B. subtilis* (Billaudeau et al. 2017).

When MreB is deleted from rod-shaped cells, the cells generally shift to more spherical forms (Margolin 2009), and coccoid bacteria have invariably lost MreB. However, some rod-shaped bacteria have also lost MreB, implying the presence of alternative methods for the maintenance of this shape. *Lactococcus lactis* lacks MreB and is typically an ovoid cell, but under certain environmental conditions cells can become rod-shaped, extending to long filaments. FtsZ is involved in these transformations (Pérez-Núñez et al. 2011). Generally, FtsZ directs the production of the cross-wall septum during cell division, playing a key role in cell division (Chapter 5), but in this case multiple rings of the division proteins develop along the filaments, with complete septation being inhibited. This kind of transition from spherical (coccoid) to rod-shaped cells has been seen in other bacteria (Lleo et al. 1990). Thus, although it has been suggested that the ancestral bacterium was rod shaped (Siefert and Fox 1998; Tamames et al. 2001), with coccoid forms being derived evolutionary dead-end states, direct evidence cautions against such a simple interpretation.

Cell Walls

Most prokaryotes, fungi, and green plants maintain their cell shapes via external support structures such as cell walls. Other forms of structural support include the scales of some chrysophytic algae, the silicious shells of diatoms, and the thecal plates of dinoflagellates. In addition to their roles in cell-shape determination, such outer coverings can play numerous other roles, such as protection against some pathogenic invaders and consumers. Structural support also allows aquatic cells to resist the turgor pressure that inevitably results from high intracellular molarity, which encourages the influx of water molecules from the environment. Cells lacking such pressure resistance would blow up without active mechanisms, such as contractile vacuoles, for continuous efflux of water. Raven (1982) makes the point that cell walls represent a one-time investment against the osmolarity problem, whereas an active mechanism of export incurs costs that must be paid throughout the life of the cell. The latter must eventually surpass the former in slower-growing cells.

One of the most striking variants of cell-wall architecture is revealed by the structural differences between Gram-negative and Gram-positive bacteria (originally identified by a difference in staining intensity of the cells). Bacterial cell walls are primarily constructed out of peptidoglycan (often called murein), a mesh of glycan chains linked together by short peptides. Gram-positive bacteria (monoderms) have a single cell membrane surrounded by a thick cell wall, whereas Gram-negative bacteria (diderms) sandwich a thin peptidoglycan layer between two lipid membranes (often with an additional layer of lipopolysaccharides on the cell surface). Although the basic structure is the same among all groups, peptidoglycans vary substantially among bacterial lineages with respect to peptide sequence, location of crosslinks between the peptide chains, and secondary modifications of the components (Vollmer and Seligman 2010).

An unsolved problem is how a dual-membrane form could have evolved from an ancestral cell with a single membrane. One hint may derive from the observation

that monoderms often produce double-membraned endospores. These are engulfed within the mother cell, such that the inner membrane of the mother becomes an external membrane enveloping the cell wall (which in turn surrounds the inner membrane) of the spore (Vollmer 2012; Tocheva et al. 2016). Some bacteria with two membranes can also produce endospores wherein the outer membrane of the maternal cell is displaced by the inner membrane (Tocheva et al. 2011). Although these observations show how a cell can undergo special kinds of divisions to establish an altered cell envelope, such changes are terminal and lost upon spore germination, so such repatterning is a far cry from demonstrating how a stable developmental pattern of two-layer biogenesis is acquired. One interpretation of the bacterial phylogeny raises the possibility that the ancestral bacterium was a sporulating diderm (with monoderms losing the outer membrane) (Tocheva et al. 2016). If correct, this is another example of the regression of complexity to more simple forms, but it leaves the origin of the diderm phenotype unexplained.

Like Gram-positive bacteria, the archaea nearly always have single lipid membranes, generally surrounded by a variant of peptidoglycan (pseudomurein) and then by an outer crystalline shell called the S layer (Albers and Meyer 2011; Visweswaran et al. 2011; Oger and Cario 2013). S layers consist of highly organized protein lattices, with substantial variation in design among species. As there is significant variation in the biosynthetic pathways leading to murein (bacteria) and pseudomurein, and little homology between the genes involved, it has been suggested that the cell walls of these two groups evolved independently (Hartmann and König 1990; Steenbakkers et al. 2006).

Although cell walls provide obvious advantages in certain ecological settings, they have been lost in most eukaryotic and some bacterial (e.g., *Mycoplasma* and *Ureaplasma*)lineages, presumably during prolonged periods in which the investment in biosynthesis outweighed the fitness advantages. Detailed calculations of the bioenergetic costs of cells walls have not yet been pursued, some simple calculations make clear that they constitute a substantial fraction of a cell's energy budget. For example Yin et al. (2007) estimate that $\sim 21\%$ of the biomass of a *S. cerevisiae* cell consists of the cell wall ($\sim 4\%$ protein, 30% mannose, 60% glycan, and 1% chitin). The glycan subunits are derived from $\sim 7.7 \times 10^9$ glucose molecules, which would otherwise be available for cellular energy or as carbon skeletons for other biosynthetic pathways, and the $\sim 1.6 \times 10^6$ protein molecules per adult cell surface constitute $\sim 2\%$ of the total protein content of the cell (Klis et al. 2014). Similar numbers were derived by Klis et al. (2014) for another yeast species, *Candida albicans.*

A more explicit statement can be made for the bacterium *E. coli.* The basic carbohydrate subunit of peptidoglycan consists of two fused molecules, NAG (N-acetylglucosamine) and NAM (N-acetylmuramic acid), with short peptide chains fused to the latter for cross-bridging. Using methods outlined in Chapter 13, the direct cost of synthesis of each peptidoglycan unit is equivalent to ~ 17 ATP hydrolyses, and the opportunity cost (associated with the lost of carbon skeletons through sugars and amino acids that otherwise could be used for energy extraction) is 206. The average surface area covered per disaccharide in this species is 2.5 nm^2, and there are $\sim 3.5 \times 10^6$ disaccharides in the entire cell wall (Wientjes et al. 1991; Gumbart et al. 2014). This suggests a total direct cost of $\sim 6 \times 10^7$ ATP hydrolyses for cell-wall biosynthesis. To put this in context, the direct costs of lipids in the cell

membrane of *E. coli* are equivalent to $\sim 8 \times 10^9$, which constitutes $\sim 28\%$ of the cell's energy requirement for growth (Chapter 16). These numbers are approximate, they suggest that the fraction of a Gram-negative bacterium's energy budget associated with the cell wall ($\sim 0.2\%$) is relative small compared to the cost of the surrounding lipid bilayers. The situation is expected to be quite different in Gram-positive bacteria, where the cell wall is greatly thickened, and there is only one lipid bilayer.

One of the most common constituents of cell walls is the concatenated polysaccharide called cellulose, a linear polymer of glucose residues, found throughout plants and even in some bacteria, and perhaps the most common biomolecule in the world. Even this simple molecule does, however, have variants among phylogenetic lineages, with the glucosyl residues sometimes carrying modified side chains.

Literature Cited

Akhmanova, A., and M. O. Steinmetz. 2015. Control of microtubule organization and dynamics: two ends in the limelight. Nat. Rev. Mol. Cell. Biol. 16: 711-726.

Albers, S. V., and K. F. Jarrell. 2018. The archaellum: an update on the unique archaeal motility structure. Trends Microbiol. 26: 351-362.

Albers, S. V., and B. H. Meyer. 2011. The archaeal cell envelope. Nat. Rev. Microbiol. 9: 414-426.

Albers, S. V., and M. Pohlschröder. 2009. Diversity of archaeal type IV pilin-like structures. Extremophiles 13: 403-410.

Alliegro, M. C., and P. Satir. 2009. Origin of the cilium: novel approaches to examine a centriolar evolution hypothesis. Methods Cell Biol. 94: 53-64.

Amir, A., F. Babaeipour, D. B. McIntosh, D. R. Nelson, and S. Jun. 2014. Bending forces plastically deform growing bacterial cell walls. Proc. Natl. Acad. Sci. USA 111: 5778-5783.

Arroyo, M., L. Heltai, D. Millán, and A. DeSimone. 2012. Reverse engineering the euglenoid movement. Proc. Natl. Acad. Sci. USA 109: 17874-17879.

Avidor-Reiss, T., A. M. Maer, E. Koundakjian, A. Polyanovsky, T. Keil, S. Subramaniam, and C. S. Zuker. 2004. Decoding cilia function: defining specialized genes required for compartmentalized cilia biogenesis. Cell 117: 527-539.

Barsanti, L., P. Coltelli, V. Evangelista, A. M. Frassanito, and P. Gualtieri. 2016. Swimming patterns of the quadriflagellate *Tetraflagellochloris mauritanica* (Chlamydomonadales, Chlorophyceae). J. Phycol. 52: 209-218.

Bazylinski, D. A., R. B. Frankel. 2004. Magnetosome formation in prokaryotes. Nat. Rev. Microbiol. 2: 217-230.

Berg, H. C. 1993. Random Walks in Biology. Princeton Univ. Press, Princeton, NJ.

Berg, H. C. 2003. The rotary motor of bacterial flagella. Annu. Rev. Biochem. 72: 19-54.

Bernander, R., and T. J. Ettema. 2010. FtsZ-less cell division in archaea and bacteria. Curr. Opin. Microbiol. 13: 747-752.

Billaudeau, C., A. Chastanet, Z. Yao, C. Cornilleau, N. Mirouze, V. Fromion, and R. Carballido-López. 2017. Contrasting mechanisms of growth in two model rod-shaped bacteria. Nat. Commun. 8: 15370.

Blocker, A., K. Komoriya, and S. Aizawa. 2003. Type III secretion systems and bacterial flagella: insights into their function from structural similarities. Proc. Natl. Acad. Sci. USA 100: 3027-3030.

Boehm, A., M. Kaiser, H. Li, C. Spangler, C. A. Kasper, M. Ackermann, V. Kaever, V. Sourjik, V. Roth, and U. Jenal. 2010. Second messenger-mediated adjustment of bacterial swimming velocity. Cell 141: 107-116.

Bratton, B. P., J. W. Shaevitz, Z. Gitai, and R. M. Morgenstein. 2018. MreB polymers and curvature localization are enhanced by RodZ and predict *E. coli*'s cylindrical uniformity. Nat. Commun. 9: 2797.

Braun, T., A. Orlova, K. Valegård, A. C. Lindås, G. F. Schröder, and E. H. Egelman. 2015. Archaeal actin from a hyperthermophile forms a single-stranded filament. Proc. Natl. Acad.

Sci. USA 112: 9340-9345.

Carlier, M. F., and S. Shekhar. 2017. Global treadmilling coordinates actin turnover and controls the size of actin networks. Nat. Rev. Mol. Cell. Biol. 18: 389-401.

Carvalho-Santos, Z., J. Azimzadeh, J. B. Pereira-Leal, and M. Bettencourt-Dias. 2011. Evolution: tracing the origins of centrioles, cilia, and flagella. J. Cell Biol. 194: 165-175.

Carvalho-Santos, Z., P. Machado, P. Branco, F. Tavares-Cadete, A. Rodrigues-Martins, J. B. Pereira-Leal, and M. Bettencourt-Dias. 2010. Stepwise evolution of the centriole-assembly pathway. J. Cell Sci. 123: 1414-1426.

Cavalier-Smith, T. 1978. The evolutionary origin and phylogeny of microtubules, mitotic spindles and eukaryote flagella. Biosystems 10: 93-114.

Cavalier-Smith, T. 2002. The phagotrophic origin of eukaryotes and phylogenetic classification of Protozoa. Internat. J. Syst. Evol. Microbiol. 52: 297-354.

Chaban, B., I. Coleman, and M. Beeby. 2018. Evolution of higher torque in *Campylobacter*-type bacterial flagellar motors. Sci. Rep. 8: 97.

Chattopadhyay, S., R. Moldovan, C. Yeung, and X. L. Wu. 2006. Swimming efficiency of bacterium *Escherichia coli.* Proc. Natl. Acad. Sci. USA 103: 13712-13717.

Chen, S., et al. 2011. Structural diversity of bacterial flagellar motors. EMBO J. 30: 2972-2981.

Chia, F.-S., J. Buckland-Nicks, and C. M. Young. 1984. Locomotion of marine invertebrate larvae: a review. Can. J. Zool. 62: 1205-1222.

Cordes, F. S., K. Komoriya, E. Larquet, S. Yang, E. H. Egelman, A. Blocker, and S. M. Lea. 2003. Helical structure of the needle of the type III secretion system of *Shigella flexneri.* J Biol Chem. 278: 17103-17107.

Crawford, D. W. 1992. Metabolic cost of motility in planktonic protists: Theoretical considerations on size scaling and swimming speed. Microb. Ecol. 24: 1-10.

Daum, B., J. Vonck, A. Bellack, P. Chaudhury, R. Reichelt, S. V. Albers, R. Rachel, and W. Kühlbrandt. 2017. Structure and *in situ* organisation of the *Pyrococcus furiosus* archaellum machinery. Elife 6: e27470.

Deng, X., G. Fink, T. A. M. Bharat, S. He, D. Kureisaite-Ciziene, and J. Löwe. 2017. Four-stranded mini microtubules formed by *Prosthecobacter* BtubAB show dynamic instability. Proc. Natl. Acad. Sci. USA 114: E5950-E5958.

Desmond, E., C. Brochier-Armanet, and S. Gribaldo. 2007. Phylogenomics of the archaeal flagellum: rare horizontal gene transfer in a unique motility structure. BMC Evol. Biol. 7: 106.

Dishinger, J. F., H. L. Kee, P. M. Jenkins, S. Fan, T. W. Hurd, J. W. Hammond, Y. N. Truong, B. Margolis, J. R. Martens, and K. J. Verhey. 2010. Ciliary entry of the kinesin-2 motor KIF17 is regulated by importin-beta2 and RanGTP. Nat. Cell Biol. 12: 703-710.

Dusenbery, D. B. 1997. Minimum size limit for useful locomotion by free-swimming microbes. Proc. Natl. Acad. Sci. USA 94: 10949-10954.

Dusenbery, D. B. 1998. Fitness landscapes for effects of shape on chemotaxis and other behaviors of bacteria. J. Bacteriol. 180: 5978-5983.

Dutcher, S. K. 2003a. Long-lost relatives reappear: identification of new members of the tubulin

superfamily. Curr. Opin. Microbiol. 6: 634-640.

Dutcher, S. K. 2003b. Elucidation of basal body and centriole functions in *Chlamydomonas reinhardtii*. Traffic 4: 443-451.

Egelman, E. H. 2010. Reducing irreducible complexity: divergence of quaternary structure and function in macromolecular assemblies. Curr. Opin. Cell Biol. 22: 68-74.

Erickson, H. P. 2007. Evolution of the cytoskeleton. Bioessays 29: 668-677.

Ettema, T. J., A. C. Lindås, and R. Bernander. 2011. An actin-based cytoskeleton in archaea. Mol. Microbiol. 80: 1052-1061.

Fenchel, T., and B. J. Finlay. 1983. Respiration rates in heterotrophic, free-living protozoa. Microb. Ecol. 9: 99122.

Ferreira, J. L., et al. 2019. γ-proteobacteria eject their polar flagella under nutrient depletion, retaining flagellar motor relic structures. PLoS Biol. 17: e3000165.

Flamholz, A., R. Phillips, and R. Milo. 2014. The quantified cell. Mol. Biol. Cell 25: 3497-3500.

Foth, B. J., M. C. Goedecke, and D. Soldati. 2006. New insights into myosin evolution and classification. Proc. Natl. Acad. Sci. USA 103: 3681-3686.

Galkin, V. E., X. Yu, J. Bielnicki, J. Heuser, C. P. Ewing, P. Guerry, and E. H. Egelman. 2008. Divergence of quaternary structures among bacterial flagellar filaments. Science 320: 382-385.

Gardner, M. K., M. Zanic, and J. Howard. 2013. Microtubule catastrophe and rescue. Curr. Opin. Cell. Biol. 25: 14-22.

Ghoshdastider, U., S. Jiang, D. Popp, and R. C. Robinson. 2015. In search of the primordial actin filament. Proc. Natl. Acad. Sci. USA 112: 9150-9151.

Ginger, M. L., N. Portman, and P. G. McKean. 2008. Swimming with protists: perception, motility and flagellum assembly. Nat. Rev. Microbiol. 6: 838-850.

Gittleson, S. M., and R. M. Noble. 1973. Locomotion in *Polytomella agilis* and *Polytoma uvella*. Trans. Amer. Micro. Soc. 92: 122-128

Gönczy, P. 2012. Towards a molecular architecture of centriole assembly. Nat. Rev. Mol. Cell Biol. 13: 425-435.

Goodson, H. V., and S. C. Dawson. 2006. Multiplying myosins. Proc. Natl. Acad. Sci. USA 103: 3498-3499.

Goodson, H. V., and W. F. Hawse. 2002. Molecular evolution of the actin family. J. Cell Sci. 115: 2619-2622.

Gumbart, J. C., M. Beeby, G. J. Jensen, and B. Roux. 2014. *Escherichia coli* peptidoglycan structure and mechanics as predicted by atomic-scale simulations. PLoS Comput. Biol. 10: e1003475.

Hariharan, V., and W. O. Hancock. 2009. Insights into the mechanical properties of the kinesin neck linker domain from sequence analysis and molecular dynamics simulations. Cell. Mol. Bioeng. 2: 177189.

Hartman, H., and T. F. Smith. 2009. The evolution of the cilium and the eukaryotic cell. Cell Motil. Cytoskeleton 66: 215-219.

Hartmann, E., and H. König. 1990. Comparison of the biosynthesis of the methanobacterial pseudomurein and the eubacterial murein. Naturwissenschaften 77: 472-475.

Hodges, M. E., N. Scheumann, B. Wickstead, J. A. Langdale, and K. Gull. 2010. Reconstructing the evolutionary history of the centriole from protein components. J. Cell Sci. 123: 1407-1413.

Horio, T., and B. R. Oakley. 1994. Human gamma-tubulin functions in fission yeast. J. Cell. Biol. 126: 1465-1473.

Hou, Y., R. Sierra, D. Bassen, N. K. Banavali, A. Habura, J. Pawlowski, and S. S. Bowser. 2013. Molecular evidence for β-tubulin neofunctionalization in Retaria (Foraminifera and radiolarians). Mol. Biol. Evol. 30: 2487-2493.

Ishikawa, H., and W. F. Marshall. 2017. Testing the time-of-flight model for flagellar length sensing. Mol. Biol. Cell. 28: 3447-3456.

Ishikawa, H., and W. F. Marshall. 2011. Ciliogenesis: building the cell's antenna. Nat. Rev. Mol. Cell Biol. 12: 222-34.

Izoré, T., D. Kureisaite-Ciziene, S. H. McLaughlin, and J. Löwe. 2016. Crenactin forms actin-like double helical filaments regulated by arcadin-2. Elife 5: e21600.

Jarrell, K. F., and M. J. McBride. 2008. The surprisingly diverse ways that prokaryotes move. Nat. Rev. Microbiol. 6: 466-476.

Jékely, G., and D. Arendt. 2006. Evolution of intraflagellar transport from coated vesicles and autogenous origin of the eukaryotic cilium. Bioessays 28: 191-198.

Joseph, J. M., P. Fey, N. Ramalingam, X. I. Liu, M. Rohlfs, A. A. Noegel, A. Müller-Taubenberger, G. Glöckner, and M. Schleicher. 2008. The actinome of *Dictyostelium discoideum* in comparison to actins and actin-related proteins from other organisms. PLoS One 3: e2654.

Kaplan, M., D. Ghosal, P. Subramanian, C. M. Oikonomou, A. Kjaer, S. Pirbadian, D. R. Ortega, A. Briegel, M. Y. El-Naggar, and G. J. Jensen. 2019. The presence and absence of periplasmic rings in bacterial flagellar motors correlates with stator type. Elife 8: e43487.

Kardon, J. R., and R. D. Vale. 2009. Regulators of the cytoplasmic dynein motor. Nat. Rev. Mol. Cell. Biol. 10: 854-865.

Katsu-Kimura, Y., F. Nakaya, S. A. Baba, and Y. Mogami. 2009. Substantial energy expenditure for locomotion in ciliates verified by means of simultaneous measurement of oxygen consumption rate and swimming speed. J. Exp. Biol. 212: 1819-1824.

Kee, H. L., J. F. Dishinger, T. L. Blasius, C. J. Liu, B. Margolis, and K. J. Verhey. 2012. A size-exclusion permeability barrier and nucleoporins characterize a ciliary pore complex that regulates transport into cilia. Nat. Cell Biol. 14: 431-437.

Kiefel, B. R., P. R. Gilson, and P. L. Beech. 2004. Diverse eukaryotes have retained mitochondrial homologues of the bacterial division protein FtsZ. Protist 155: 105-115.

Kinosita, Y., N. Uchida, D. Nakane, and T. Nishizaka. 2016. Direct observation of rotation and steps of the archaellum in the swimming halophilic archaeon *Halobacterium salinarum.* Nat. Microbiol. 1: 16148.

Klis, F. M., C. G. de Koster, and S. Brul. 2014. Cell wall-related bionumbers and bioestimates of *Saccharomyces cerevisiae* and *Candida albicans.* Eukaryot. Cell 13: 2-9.

Kulak, N. A., G. Pichler, I. Paron, N. Nagaraj, and M. Mann. 2014. Minimal, encapsulated proteomic-sample processing applied to copy-number estimation in eukaryotic cells. Nat. Methods 11: 319-324.

Kull, F. J., R. D. Vale, and R. J. Fletterick. 1998. The case for a common ancestor: kinesin and myosin motor proteins and G proteins. J. Muscle Res. Cell Motil. 19: 877-886.

Lassak, K., T. Neiner, A. Ghosh, A. Klingl, R. Wirth, and S. V. Albers. 2012. Molecular analysis of the crenarchaeal flagellum. Mol. Microbiol. 83: 110-124.

Liu, R., and H. Ochman. 2007. Stepwise formation of the bacterial flagellar system. Proc. Natl. Acad. Sci. USA 104: 7116-7121.

Lleo, M. M., P. Canepari, and G. Satta. 1990. Bacterial cell shape regulation: testing of additional predictions unique to the two-competing-sites model for peptidoglycan assembly and isolation of conditional rod-shaped mutants from some wild-type cocci. J. Bacteriol. 172: 3758-3771.

Lovely, P. S., and F. W. Dahlquist. 1975. Statistical measures of bacterial motility and chemotaxis. J. Theor. Biol. 50: 477-496.

Löwe, J., and L. A. Amos. 2009. Evolution of cytomotive filaments: the cytoskeleton from prokaryotes to eukaryotes. Int. J. Biochem. Cell Biol. 41: 323-329.

Lu, P., C. Vogel, R. Wang, X. Yao, and E. M. Marcotte. 2007. Absolute protein expression profiling estimates the relative contributions of transcriptional and translational regulation. Nat. Biotechnol. 25: 117-124.

Ludington, W. B., L. Z. Shi, Q. Zhu, M. W. Berns, and W. F. Marshall. 2012. Organelle size equalization by a constitutive process. Curr. Biol. 22: 2173-2179.

Ludington, W. B., K. A. Wemmer, K. F. Lechtreck, G. B. Witman, and W. F. Marshall. 2013. Avalanche-like behavior in ciliary import. Proc. Natl. Acad. Sci. USA 110: 3925-30.

Lynch, M., and G. K. Marinov. 2015. The bioenergetic costs of a gene. Proc. Natl. Acad. Sci. USA 112: 15690-15695.

Maezawa, K., S. Shigenobu, H. Taniguchi, T. Kubo, S. Aizawa, and M. Morioka. 2006. Hundreds of flagellar basal bodies cover the cell surface of the endosymbiotic bacterium *Buchnera aphidicola* sp. strain APS. J. Bacteriol. 188: 6539-6543.

Makarova, K. S., N. Yutin, S. D. Bell, and E. V. Koonin. 2010. Evolution of diverse cell division and vesicle formation systems in Archaea. Nat. Rev. Microbiol. 8: 731-741.

Männik, J., R. Driessen, P. Galajda, J. E. Keymer, and C. Dekker. 2009. Bacterial growth and motility in sub-micron constrictions. Proc. Natl. Acad. Sci. USA 106: 14861-14866.

Manson, M. D., P. M. Tedesco, and H. C. Berg. 1980. Energetics of flagellar rotation in bacteria. J. Mol. Biol. 138: 541-561.

Manson, M. D., P. Tedesco, H. C. Berg, F. M. Harold, and C. Van der Drift. 1977. A proton motive force drives bacterial flagella. Proc. Natl. Acad. Sci. USA 74: 3060-3064.

Margolin, W. 2009. Sculpting the bacterial cell. Curr. Biol. 19: R812-R822.

Marguerat, S., A. Schmidt, S. Codlin, W. Chen, R. Aebersold, and J. Bähler. 2012. Quantitative analysis of fission yeast transcriptomes and proteomes in proliferating and quiescent cells. Cell 151: 671-683.

Marshall, W. F., and J. L. Rosenbaum. 2001. Intraflagellar transport balances continuous turnover of outer doublet microtubules: implications for flagellar length control. J. Cell Biol. 155: 405-414.

Mast, F. D., R. A. Rachubinski, and J. B. Dacks. 2012. Emergent complexity in myosin V-based organelle inheritance. Mol. Biol. Evol. 29: 975-984.

McKean, P. G., S. Vaughan, and K. Gull. 2001. The extended tubulin superfamily. J. Cell Sci. 114: 2723-2733.

Meister, M., G. Lowe, and H. C. Berg. 1987. The proton flux through the bacterial flagellar motor. Cell 49: 643-650.

Michie, K. A., and J. Löwe. 2006. Dynamic filaments of the bacterial cytoskeleton. Annu. Rev. Biochem. 75: 467-492.

Monds, R. D., T. K. Lee, A. Colavin, T. Ursell, S. Quan, T. F. Cooper, and K. C. Huang. 2014. Systematic perturbation of cytoskeletal function reveals a linear scaling relationship between cell geometry and fitness. Cell Rep. 9: 1528-1537.

Nan, B., and D. R. Zusman. 2016. Novel mechanisms power bacterial gliding motility. Mol. Microbiol. 101: 186-193.

Norbeck, J., and A. Blomberg. 1997. Two-dimensional electrophoretic separation of yeast proteins using a non-linear wide range (pH 3-10) immobilized pH gradient in the first dimension; reproducibility and evidence for isoelectric focusing of alkaline (pI ¿ 7) proteins. Yeast 13: 1519-1534.

Oger, P. M., and A. Cario. 2013. Adaptation of the membrane in Archaea. Biophys. Chem. 183: 42-56.

Osawa, M., and H. P. Erickson. 2006. FtsZ from divergent foreign bacteria can function for cell division in *Escherichia coli.* J. Bacteriol. 188: 7132-7140.

Ouzounov, N., J. P. Nguyen, B. P. Bratton, D. Jacobowitz, Z. Gitai, and J. W. Shaevitz. 2016. MreB orientation correlates with cell diameter in *Escherichia coli.* Biophys. J. 111: 1035-1043.

Ozyamak, E., J. M. Kollman, and A. Komeili. 2013. Bacterial actins and their diversity. Biochemistry 52: 6928-6939.

Pallen, M. J., and N. J. Matzke. 2006. From The Origin of Species to the origin of bacterial flagella. Nat. Rev. Microbiol. 4: 784-790.

Pallen, M. J., C. W. Penn, and R. R. Chaudhuri. 2005. Bacterial flagellar diversity in the post-genomic era. Trends Microbiol. 13: 143-149.

Pazour, G. J., N. Agrin, J. Leszyk, and G. B. Witman. 2005. Proteomic analysis of a eukaryotic cilium. J. Cell. Biol. 170: 103-113.

Pérez-Núñez, D., R. Briandet, B. David, C. Gautier, P. Renault, B. Hallet, P. Hols, R. Carballido-López, and E. Guédon. 2011. A new morphogenesis pathway in bacteria: unbalanced activity of cell wall synthesis machineries leads to coccus-to-rod transition and filamentation in ovococci. Mol. Microbiol. 79: 759-771.

Perrin, F. 1934. Mouvement Brownien d'un ellipsoide. I. Dispersion dilectrique pour des molécules ellipsoidales. J. Phys. Radium 5: 497-511.

Perrin, F. 1936. Mouvement Brownien d'un ellipsoide. II. Rotation libre et dépolarisation des fluorescences. Translation et diffusion de molécules ellipsoidales. J. Phys. Radium 7: 1-11.

Pilhofer, M., M. S. Ladinsky, A. W. McDowall, G. Petroni, and G. J. Jensen. 2011. Microtubules in bacteria: ancient tubulins build a five-protofilament homolog of the eukaryotic cytoskeleton. PLoS Biol. 9: e1001213.

Pla, J., M. Sanchez, P. Palacios, M. Vicente, and M. Aldea. 1991. Preferential cytoplasmic location of FtsZ, a protein essential for *Escherichia coli* septation. Mol. Microbiol. 5: 1681-1686.

Purcell, E. M. 1977. Life at low Reynolds number. Amer. J. Physics 45: 311.

Quintero, O. A., and C. M. Yengo. 2012. Myosin X dimerization and its impact on cellular functions. Proc. Natl. Acad. Sci. USA 109: 17313-17314.

Raven, J. A., and K. Richardson. 1984. Dinophyte flagella: a cost-benefit analysis. New Phytol. 98: 259-276

Richards, T. A., et al. 2004. A standardized kinesin nomenclature. J. Cell Biol. 167: 19-22.

Rosenbaum, J. L., and G. B. Witman. 2002. Intraflagellar transport. Nat. Rev. Mol. Cell Biol. 3: 813-825.

Ross, L., and B. B. Normark. 2015. Evolutionary problems in centrosome and centriole biology. J. Evol. Biol. 28: 995-1004.

Rossmann, F. M., and M. Beeby. 2018. Insights into the evolution of bacterial flagellar motors from high-throughput *in situ* electron cryotomography and subtomogram averaging. Acta Crystallogr. D Struct. Biol. 74: 585-594.

Rueda, S., M. Vicente, and J. Mingorance. 2003. Concentration and assembly of the division ring proteins FtsZ, FtsA, and ZipA during the *Escherichia coli* cell cycle. J. Bacteriol. 185: 3344-3351.

Salje, J., P. Gayathri, and J. Löwe. 2010. The ParMRC system: molecular mechanisms of plasmid segregation by actin-like filaments. Nat. Rev. Microbiol. 8: 683-692.

Satir, P., C. Guerra, and A. J. Bell. 2007. Evolution and persistence of the cilium. Cell Motil. Cytoskeleton 64: 906-913.

Sato, K., et al. 2007. Stroke frequency, but not swimming speed, is related to body size in free-ranging seabirds, pinnipeds and cetaceans. Proc. Biol. Sci. 274: 471-477.

Scholey, J. M. 2013. Kinesin-2: a family of heterotrimeric and homodimeric motors with diverse intracellular transport functions. Annu. Rev. Cell Dev. Biol. 29: 443-469.

Schwanhäusser, B., D. Busse, N. Li, G. Dittmar, J. Schuchhardt, J. Wolf, W. Chen, and M. Selbach. 2011. Global quantification of mammalian gene expression control. Nature 473: 337-342.

Sehring, I. M., C. Reiner, J. Mansfeld, H. Plattner, and R. Kissmehl. 2007. A broad spectrum of actin paralogs in *Paramecium tetraurelia* cells display differential localization and function. J. Cell Sci. 120: 177-190.

Shastry, S., and W. O. Hancock. 2010. Neck linker length determines the degree of processivity in kinesin-1 and kinesin-2 motors. Curr. Biol. 20: 939-943.

Siefert, J. L., and G. E. Fox. 1998. Phylogenetic mapping of bacterial morphology. Microbiology 144: 2803-2808.

Smith, J. C., J. G. Northey, J. Garg, R. E. Pearlman, and K. W. Siu. 2005. Robust method for proteome analysis by MS/MS using an entire translated genome: demonstration on the ciliome of *Tetrahymena thermophila.* J. Proteome Res. 4: 909-919.

Sosinsky, G. E., N. R. Francis, D. J. DeRosier, J. S. Wall, M. N. Simon, and J. Hainfeld. 1992. Mass determination and estimation of subunit stoichiometry of the bacterial hook-basal body flagellar complex of *Salmonella typhimurium* by scanning transmission electron microscopy. Proc. Natl. Acad. Sci. USA 89: 4801-4805.

Steenbakkers, P. J., W. J. Geerts, N. A. Ayman-Oz, and J. T. Keltjens. 2006. Identification of pseudomurein cell wall binding domains. Mol. Microbiol. 62: 1618-1630.

Stepanek, L., and G. Pigino. 2016. Microtubule doublets are double-track railways for intraflagellar transport trains. Science 352: 721-724.

Snyder, L. A., N. J. Loman, K. Fütterer, and M. J. Pallen. 2009. Bacterial flagellar diversity and evolution: seek simplicity and distrust it? Trends Microbiol. 17: 1-5.

Tam, D., and A. E. Hosoi. 2011. Optimal feeding and swimming gaits of biflagellated organisms. Proc. Natl. Acad. Sci. USA 108: 1001-1006.

Tamames, J., M. Gonzalez-Moreno, J. Mingorance, A. Valencia, and M. Vicente. 2001. Bringing gene order into bacterial shape. Trends Genet. 17: 124-126.

Taniguchi, Y., P. J. Choi, G. W. Li, H. Chen, M. Babu, J. Hearn, A. Emili, and X. S. Xie. 2010. Quantifying *E. coli* proteome and transcriptome with single-molecule sensitivity in single cells. Science 329: 533-538.

Taylor TB, Mulley G, Dills AH, Alsohim AS, McGuffin LJ, Studholme DJ, Silby MW, Brockhurst MA, Johnson LJ, Jackson RW. 2015. Evolutionary resurrection of flagellar motility via rewiring of the nitrogen regulation system. Science 347: 1014-1017.

Thomas, N. A., S. L. Bardy, and K. F. Jarrell. 2001. The archaeal flagellum: a different kind of prokaryotic motility structure. FEMS Microbiol. Rev. 25: 147-174.

Tocheva, E. I., E. G. Matson, D. M. Morris, F. Moussavi, J. R. Leadbetter, and G. J. Jensen. 2011. Peptidoglycan remodeling and conversion of an inner membrane into an outer membrane during sporulation. Cell 146: 799-812.

Tocheva, E. I., D. R. Ortega, and G. J. Jensen. 2016. Sporulation, bacterial cell envelopes and the origin of life. Nat. Rev. Microbiol. 14: 535-542.

Toft, C., and M. A. Fares. 2008. The evolution of the flagellar assembly pathway in endosymbiotic bacterial genomes. Mol. Biol. Evol. 25: 2069-2076.

Typas, A., M. Banzhaf, C. A. Gross, and W. Vollmer. 2011. From the regulation of peptidoglycan synthesis to bacterial growth and morphology. Nat. Rev. Microbiol. 10: 123-136.

Ursell, T. S., J. Nguyen, R. D. Monds, A. Colavin, G. Billings, N. Ouzounov, Z. Gitai, J. W. Shaevitz, and K. C. Huang. 2014. Rod-like bacterial shape is maintained by feedback between cell curvature and cytoskeletal localization. Proc. Natl. Acad. Sci. USA 111: E1025-E1034.

van Dam, T. J., M. J. Townsend, M. Turk, A. Schlessinger, A. Sali, M. C. Field, and M. A. Huynen. 2013. Evolution of modular intraflagellar transport from a coatomer-like progenitor. Proc. Natl. Acad. Sci. USA 110: 6943-6948.

van Niftrik, L., et al. 2009. Cell division ring, a new cell division protein and vertical inheritance

of a bacterial organelle in anammox planctomycetes. Mol. Microbiol. 73: 1009-1019.

Vischer, N. O., et al. 2015. Cell age dependent concentration of *Escherichia coli* divisome proteins analyzed with ImageJ and ObjectJ. Front. Microbiol. 6: 586.

Visweswaran, G. R., B. W. Dijkstra, and J. Kok. 2011. Murein and pseudomurein cell wall binding domains of bacteria and archaea – a comparative view. Appl. Microbiol. Biotechnol. 92: 921-928.

Vollmer, W., and S. J. Seligman. 2010. Architecture of peptidoglycan: more data and more models. Trends Microbiol. 18: 59-66.

Wagstaff, J., and J. Löwe. 2018. Prokaryotic cytoskeletons: protein filaments organizing small cells. Nat. Rev. Microbiol. 16: 187-201.

Walter, W. J., and S. Diez. 2012. Molecular motors: a staggering giant. Nature 482: 44-45.

Walsby, A. E. 1994. Gas vesicles. Microbiol. Rev. 58: 94-144.

Wang, S., L. Furchtgott, K. C. Huang, and J. W. Shaevitz. 2012. Helical insertion of peptidoglycan produces chiral ordering of the bacterial cell wall. Proc. Natl. Acad. Sci. USA 109: E595-604.

Waterbury, J. B., J. M. Willey, D. G. Franks, F. W. Valois, and S. W. Watson. 1985. A cyanobacterium capable of swimming motility. Science 230: 74-76.

Wickstead, B., and K. Gull. 2007. Dyneins across eukaryotes: a comparative genomic analysis. Traffic 8: 1708-1721.

Wickstead, B., and K. Gull. 2011. The evolution of the cytoskeleton. J. Cell Biol. 194: 513-525.

Wickstead, B., K. Gull, and T. A. Richards. 2010. Patterns of kinesin evolution reveal a complex ancestral eukaryote with a multifunctional cytoskeleton. BMC Evol. Biol. 10: 110.

Wientjes, F. B., C. L. Woldringh, and N. Nanninga. 1991. Amount of peptidoglycan in cell walls of gram-negative bacteria. J. Bacteriol. 173: 7684-7691.

Wilkes, D. E., H. E. Watson, D. R. Mitchell, and D. J. Asai. 2008. Twenty-five dyneins in *Tetrahymena:* a re-examination of the multidynein hypothesis. Cell Motil. Cytoskeleton 65: 342-351.

Wisniewski, J. R., and D. Rakus. 2014. Quantitative analysis of the *Escherichia coli* proteome. Data Brief 1: 7-11.

Wu, J. Q., and T. D. Pollard. 2005. Counting cytokinesis proteins globally and locally in fission yeast. Science 310: 310-314.

Yin, Q. Y., P. W. de Groot, L. de Jong, F. M. Klis, and C. G. De Koster. 2007. Mass spectrometric quantitation of covalently bound cell wall proteins in *Saccharomyces cerevisiae.* FEMS Yeast Res. 7: 887-896.

Young, K. D. 2006. The selective value of bacterial shape. Microbiol. Mol. Biol. Rev. 70: 660-703.

Young, K. D. 2010. Bacterial shape: two-dimensional questions and possibilities. Annu. Rev. Microbiol. 64: 223-240.

Zhang, P., W. Dai, J. Hahn, and S. P. Gilbert. 2015. *Drosophila* Ncd reveals an evolutionarily conserved powerstroke mechanism for homodimeric and heterodimeric kinesin-14s. Proc. Natl. Acad. Sci. USA 112: 6359-6364.

Figure 15.1. Examples of the three key forms of fibril-forming proteins in eukaryotes. Individual tubulin filaments are comprised of heterodimers of two elemental forms of tubulin. Intermediate filaments can assemble into higher-order structures such as cables and sheets.

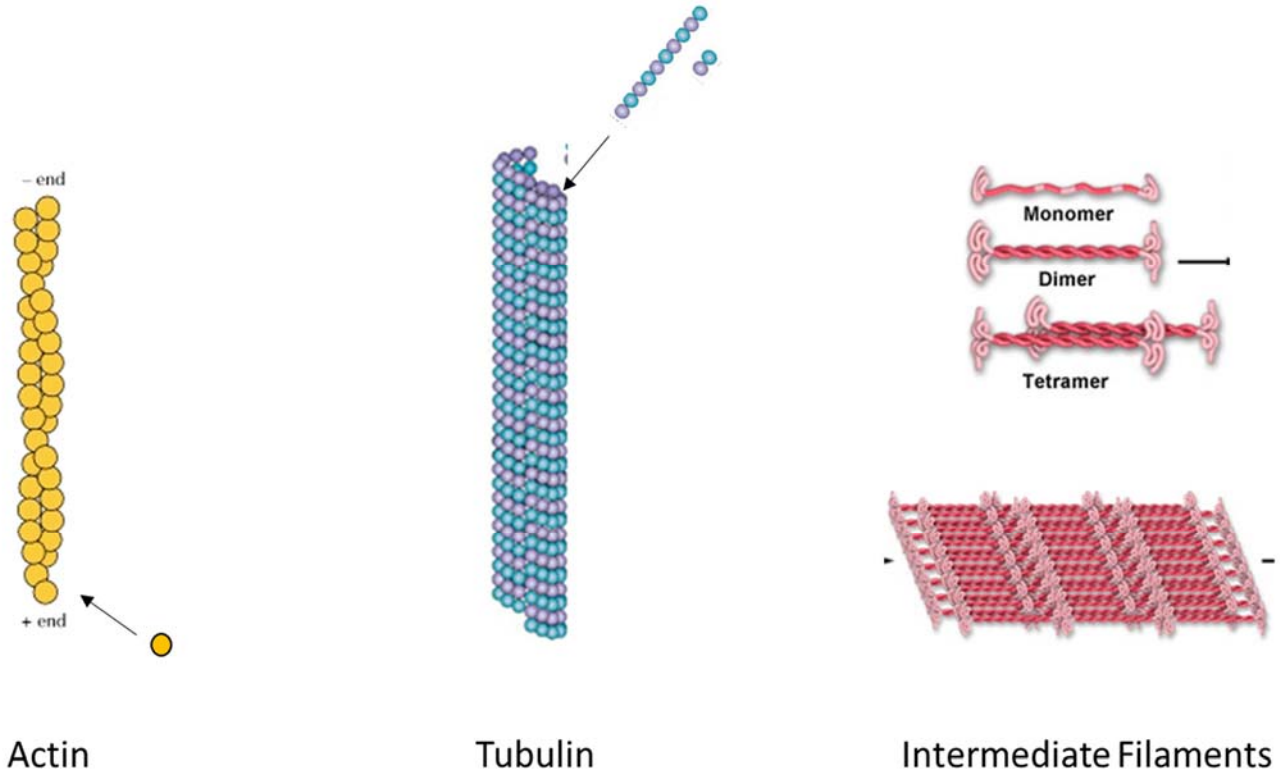

Figure 15.2. An example of a motor protein interfacing with a microtubule, along which it walks fueled by energy derived from ATP hydrolysis, carrying its cargo (in this case a transport vesicle).

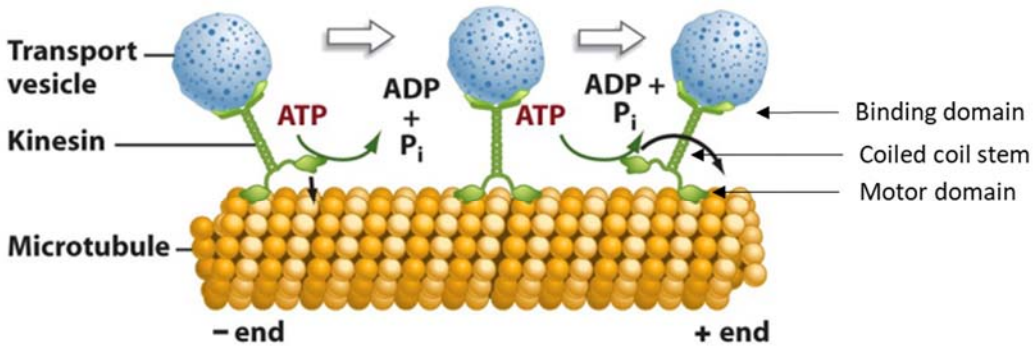

Figure 15.3. Idealized schematics of bacterial (left) and eukaryotic (right) flagella. The former emanates from a complex apparatus embedded in the double membrane. The latter grows out of a basal body (centriole), and has an interior consisting of tubulins along which motor proteins move.

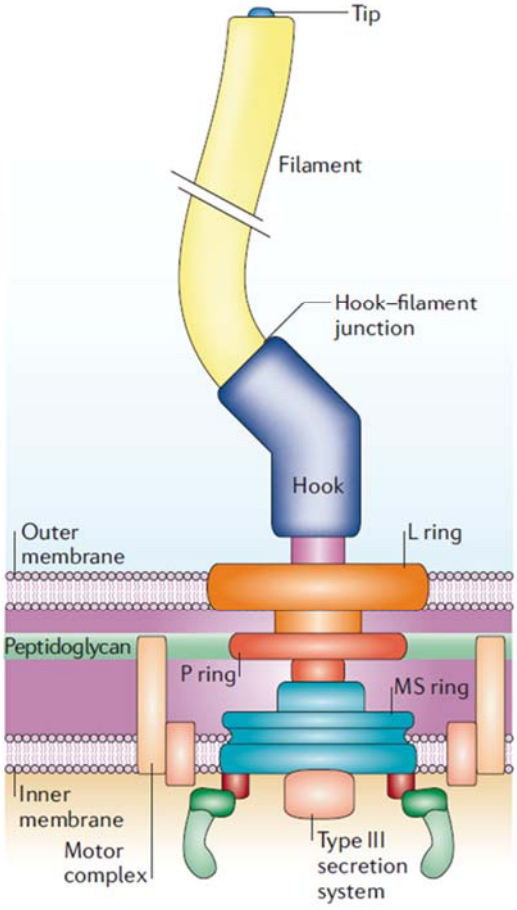

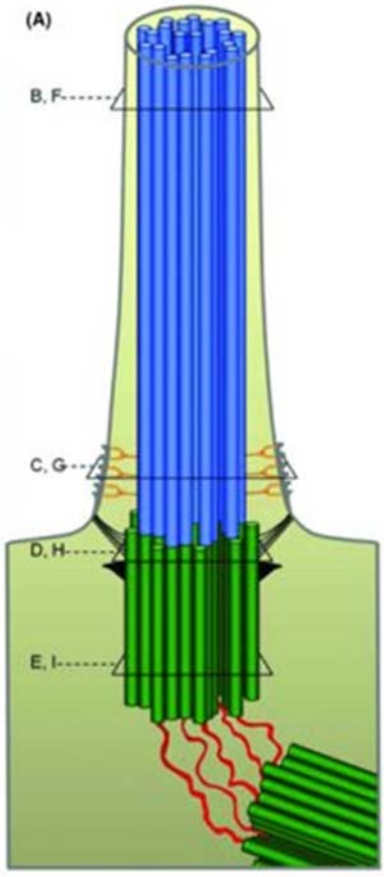

Figure 15.4. Scaling relationships between swimming velocities (v) and cell volume (V) in unicellular species. For eukaryotes, $v = 10.5V^{0.30}$, $r^2 = 0.49$); and for bacteria, $v = 27.8V^{0.19}$, $r^2 = 0.21$). The measured values are corrected for temperature assuming a Q10 of 2.0.

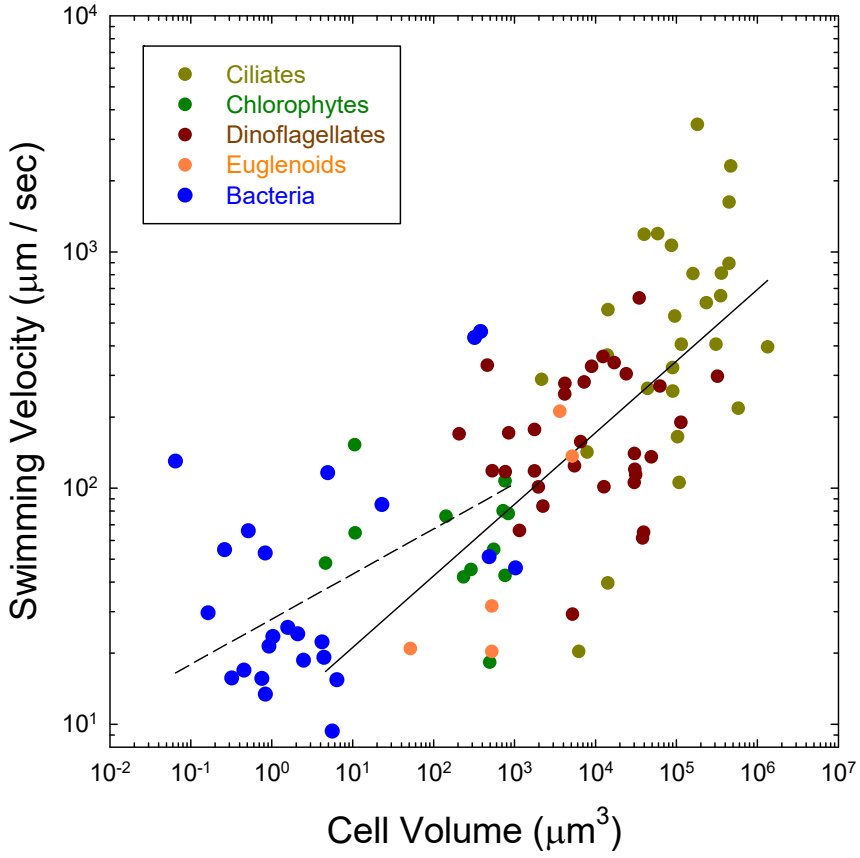

Figure 15.5. A cartoon version of a peptidoglycan layer. The paired hexagons represent dimers of NAM and NAG, whereas the small chains represent cross-linked peptides.